UNIVERSITY OF CALIFORNIA
SANTA CRUZ

THERMOELECTRICS COMBINED WITH SOLAR CONCENTRATION FOR ELECTRICAL AND THERMAL COGENERATION

A thesis submitted in partial satisfaction
of the requirements for the degree of

MASTER OF SCIENCE

in

ELECTRICAL ENGINEERING

by

Philip Jackson

September 2012

The Thesis of Philip Jackson

is approved:

_____
Professor Ali Shakouri, Chair

_____
Professor Joel Kubby

_____
Professor Holger Schmidt

_____
Tyrus Miller
Vice Provost and Dean of Graduate Studies

TABLE OF CONTENTS

LIST OF FIGURES

ABSTRACT

PHILIP JACKSON

THERMOELECTRICS COMBINED WITH SOLAR CONCENTRATION FOR ELECTRICAL AND THERMAL COGENERATION

A solar tracker and concentrator was designed and assembled for the purpose of cogeneration of thermal power and electrical power using thermoelectric technology. A BiTe thermoelectric module was placed between the concentrated sunlight and a water cooling system to produce electrical power from the temperature gradient. The system was tested with the intent of determining if thermoelectric devices could provide beneficial synergy to solar thermal systems. The system was able to transfer 78% of the incident 384 watts of thermal energy from the sun via the water cooling system, but was not able to produce a substantial amount of electrical power with the thermoelectric module. The TE module only performed at 15% of its expected output of 3 watts. Either the modules were not as powerful as advertised or the thermal impedances of the various layers within the receiver were not well matched for optimal heat transport. The closed loop water cooling system worked well to display how well the system can extract thermal energy from the receiver, but the system was not well designed for optimal thermal storage after extracting the heat. Additional studies were done for optimizing the system performance, such as the effect of concentrator misalignment on the receiver output, as well as the introduction of absorbing coatings on the receiver for increased output. After preliminary testing,

simulations and modifications to the system were performed in order to prevent receiver overheating and optimize system performance. Further system improvements are discussed, in addition to future investigations that would be useful for advancing sustainable energy solutions.

ACKNOWLEDGEMENTS

I would like to express my gratitude to the following people/entities for helping me through this project and my time at UC Santa Cruz with support, guidance, discussions, and funding.

I am greatly indebted to Professor Ali Shakouri, for sparking my initial interest in graduate school studying renewable energy and sustainability. He has given me great insight into the world of academic research and has helped me develop research skills and habits that will benefit me for the rest of my career. His extensive support, motivation, and guidance through this process have made this project and many others successful. Thank you!

I wish to thank the members of my thesis review committee, Professors Ali Shakouri, John Vesecky, and Joel Kubby, for taking the time to review my thesis and providing constructive comments and suggestions for improving my content.

I am very thankful to Zhixi Bian, Kazuaki Yazawa, and Vernon Wong for many constructive conversations about the theory and execution of my experiment. Kaz and Vernon worked on a similar project and they suggested many interesting experiments and techniques that proved very helpful. I would also like to thank all the Professors that I had graduate level classes with: Ali, Shakouri, Holger Schmidt, Nobby

Kobayashi, Joel Kubby, and Mike Issacson, for giving me a great deal of knowledge that has helped me get to this point.

I would like to strongly acknowledge the contributions of Dave Thayer and Darryl Smith at the Baskin Engineering machine shop, for providing many hours assisting me with the design, assembly, and maintenance of the tracking frame. Without their contributions, the project would not have gotten underway in the first place.

I would like to express my appreciation to DARPA/Army for providing Ali and myself with the funding necessary to complete this project. Without their financial support, none of this would have been possible. I would also like to acknowledge all the administrators and assistants that have assisted me during my time at UCSC with all the management level tasks: Robert Vitale, Jeff Duncan, Robert Spurgeon, Brenna Candelaria, Tammy Tooley-Chelossi, Frances Ruiz-Wood, Carol Mullane, Jolinda Singleton, and Cynthia McCarley.

I would also like to express my appreciation to all the members of the Quantum Electronics Group at UC Santa Cruz that I had the opportunity to work with for the past four years: Ali Shakouri, Zhixi Bian, Kazuaki Yazawa, Rajeev Singh, James Christofferson, Kerry Maize, Mona Zebarjadi, Xi Wang, Tela Favaloro, Paul Abumov, Shila Alavi, Bjorn Veermersch, Gilles Pernot, Helene Michel, Dustin Kendig, Younes Ezzahri, Oxana Pantchenko, Takehiro Onishi, Amirkoushyar

Ziabari, Ramin Banan-Sadeghian, Je-Hyeong Bahk, Ekaterina Selezneva, Je-Hyoung Park, Yeerui Koh, Amr Mohammed, Carolina Carmo, Alireza Rezaniakolaei, Daniel Hernandez, Carol Owens, George Weickhardt, Salvador Vazquez, Danny Tate, Vernon Wong, and Ruben Chavez. You have all been a great group to work with and I wish you all the best as you progress through your careers and lives.

Finally, I would like to express my deepest gratitude to my family for supporting me throughout this process. My father, Eric Jackson; My mother, Sheryl Rives; my brother, Daniel Jackson, my loving and supportive partner, Catherine Olivier, and all my other friends and family members that have all been instrumental in my success up to this point in my life. I love you all and appreciate your never-ending support.

Santa Cruz, CA,

August 2012

Philip Jackson

1. Motivation

As human civilization has advanced over the decades, the need for more energy has greatly increased. At present, the world has a substantial reliance on energy originating from fossil fuels, such as coal and petroleum, due to the high energy yield of these resources for relatively low cost. A barrel of crude oil, which cost $95 per barrel on average during 2011, contains 1700 kilowatt-hours (kWh) of energy, which translates to $0.06 per kWh. Comparatively, in 2012, a 5 kW solar panel array costing $17,000, operating 20 years and getting an average peak solar exposure of 3.6 hours a day will yield $0.14 per kWh. In comparison to 2009, the contrast between these two resources was much greater, with $0.04 per kWh for oil ($62/barrel) versus $0.24 per kWh for solar, as solar systems were much more expensive ($29,000 per 5 kW system). Although we have an economic incentive to continue using oil, the process of extracting energy from fossil fuels generates greenhouse gases, which can lead to adverse effects on air quality, ocean acidity, and global climate change. However, despite these environmental concerns, the economies of the world continue to develop and expand their dependency on oil.

The American economy has become dangerously subservient to its heavy dependence on fossil fuels. The availability of oil has a strong influence on the country's foreign policy decisions and economy. The price of oil in the world market has steadily risen as a result of increased demand from developing economies in countries like India and China, in addition to large occasional spikes in oil prices as a

result of global events, such as the 1973 Oil Embargo that occurred as a result of the US supporting Israel in the Yom Kippur War. According to statistics collected by the CIA, the United States consumed an average of 18.7 million barrels of crude oil per day in 2009, which was 22% of the world's total oil usage. With other countries increasing their oil needs, the U.S. needs to be concerned with possible strain on foreign relations with oil suppliers and with consumption competitors. If other countries in the world begin to use as much oil as the United States does, the insufficient supply will cause oil prices to reach astronomical levels. Alternative means of energy generation will be very important for global stability and self sustainability in the coming decades.

Renewable energy generation has not been sufficiently implemented into the country's energy infrastructure. Every few years, Lawrence Livermore National Laboratory performs a study on the estimated energy usage of the United States in a given year. The research investigates which resources supply America's energy (Coal, biomass, etc.), in addition to where that energy is used (residential, commercial, etc.) and how much of the used energy is lost in the form of heat. Figure 1.1 below is a flow chart that presents their findings for the year 2009. This data shows that the United States used approximately 95 Quads of energy in 2009, where a quad is an equivalent amount of energy as eight billion gallons of gasoline. 83% of the country's energy originated from fossil fuels, and of all the energy used, 58% of the energy is rejected in the form of heat. Energy generated by renewable technology, such as wind and solar, is rather insubstantial. In comparison to a similar study

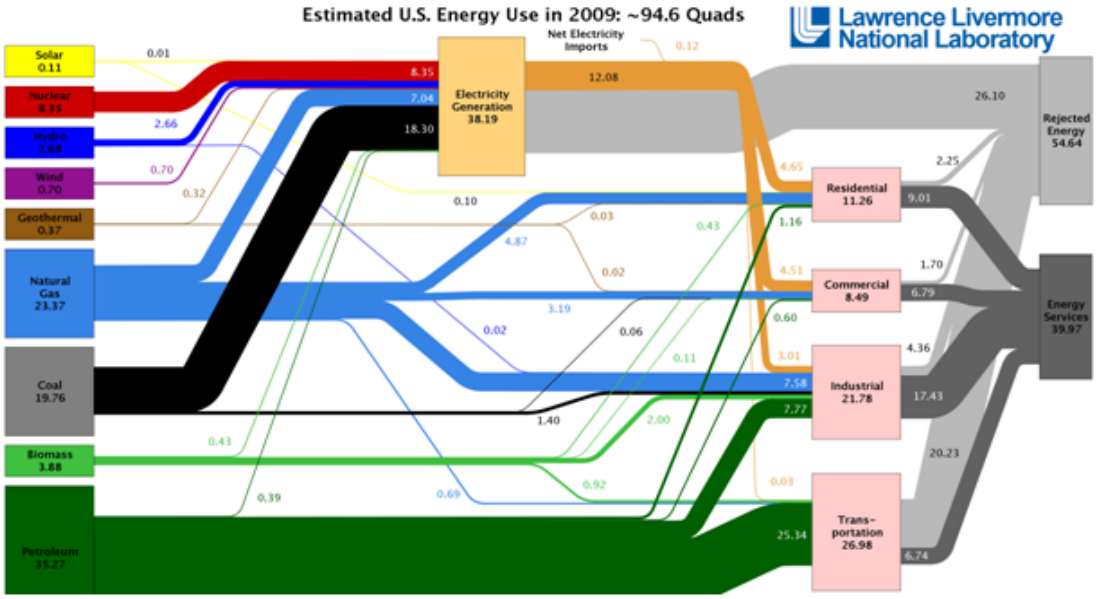

Figure 1.1: US energy flow trends for 2009.

performed in 2002, energy usage went down slightly, specifically from fossil fuel resources, but the rejected energy remained the same. Despite population growth between these years (U.S. Census Bureau has observed an average growth of 3 million people per year), energy usage remained relatively constant. These trends suggest that public awareness of reducing energy usage has improved, but our technological advances have not improved overall system efficiencies. While these trends are beginning to shift in a promising direction, the rate of progress is troubling for the future of the country if self sustainability it to be achieved.

The goal of this project was to investigate several forms of renewable energy, specifically solar concentration and thermoelectric materials, and evaluate the energy generation potential when these technologies are combined. By producing an

experiment that reflects the useful applications of renewable technology, my hope is to gain sufficient understanding of both technologies so I can contribute further to this field and help to secure our energy future. In short, thermoelectric materials generate an electrical current from a temperature gradient across the material. For this experiment, a solar concentration system was used to heat one side of the thermoelectric material to establish the hot side temperature, while water cooling was used to maintain the cold side temperature. The solar concentrator, tracking, and cooling system were designed and assembled for optimal power generation and system efficiency tests, as well as maximizing the thermal energy carried away from the receiver. In addition, software was written using LabView for automated data acquisition and recording. The data was analyzed to evaluate how efficiently the system could cogenerate electrical power and hot water for thermal storage.

2. Theory and Background

Before explaining the design and results of the project, it is important to explain the theory that governs the experiment. This section is designed to explain all the information a person outside this field of research would need in order to understand and perform similar experiments. I will explain the theory behind thermoelectric materials, solar thermal, cogeneration of electrical and thermal energy, and the software used for this project called LabView and ANSYS.

2.1. Thermoelectrics

The Thermoelectric Effect describes the direct conversion of electrical potential to a temperature gradient in an electrically conductive material. Thermoelectric devices are typically used for generating power from temperature differences and cooling or heating devices using a voltage. The broad name of the "Thermoelectric Effect" includes several separate phenomena, including the Seebeck Effect, Peltier Effect, and Thomson Effect, which are all used to explain the behavior of thermoelectrics.

2.1.1. Seebeck Effect

Whenever a temperature gradient exists across an electrically conductive material, a potential difference will also exist between two points at different temperatures along that gradient. Since electrons try to minimize their energy, this results in the electrons' tendency to migrate from high energy areas (hot) to lower energy areas (cold). This phenomenon was first observed by Thomas Johann Seebeck in 1823, and is referred to as the Seebeck Effect. The relationship between the voltage produced by a given temperature difference is:

$$S = \frac{-\Delta V}{\Delta T}$$

where V is the potential difference between two points along the gradient, T is the temperature difference between the same two points, and S is the material's Seebeck coefficient. A negative Seebeck Coefficient corresponds to a n-type semiconductor,

where electrons are the dominant charge carrier. The magnitude of a good thermoelectric material's Seebeck Coefficient is on the order of 100 μV/K. BiTe thin films were grown in 2005 by J. Tan et al, which possessed a Seebeck coefficient of -287 uV/K. When an electrical load is connected in series with an electrical conductor with a temperature gradient, current will flow through the load. Conversely, if a voltage is created across a conductor, a temperature difference will be created.

2.1.2. Peltier Effect

When current is sent through a junction of two dissimilar materials, a change in the junction's temperature will occur. This phenomenon was named the Peltier Effect after it was first observed by Jean-Charles Peltier in 1834. This idea was further expanded by Heinrich Lenz in 1838, when he observed that the temperature of the junction will either increase or decrease, depending on the direction in which the current travels. The rate at which heat is emitted or absorbed is:

$$Q = \prod I$$

where I is the current applied and π is the Peltier Coefficient, which can be described as the average thermal energy carried per unit charge. In the case of an n-type semiconductor and a metal, Figure 2.1 below shows the thermoelectric interaction for when electrons travel from the metal into the semiconductor. The diagram shows the ohmic contact of a metal and an n-type semiconductor. As the electrons move into the

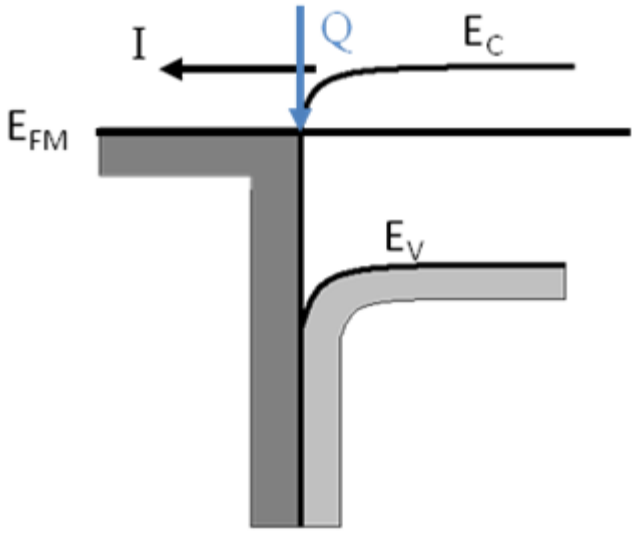

Figure 2.1: Energy diagram of an ohmic contact (metal to n-type).

conduction band of the semiconductor, they must absorb energy from the lattice. If the current direction is reversed, then the electrons flow into a lower energy levels and release heat at the junction.

2.1.3. Thomson Effect

The Thomson Effect was first observed by William Thomson in 1851. He described how heating or cooling would occur in a current-carrying conductor with a temperature gradient. Any current-carrying conductor, with the exception of superconductors, with a temperature gradient existing between two points will either absorb or emit heat. If a current density J is travelling through a homogeneous conductor, the generated heat q per unit volume is:

$$q = \rho J^2 - \mu J \frac{dT}{dx}$$

where ρ is the resistivity of the material, μ is the Thomson Coefficient, and dT/dx is the temperature gradient along the conductor. The first term corresponds to the Joule heating, which will always be positive, while the second term is the Thomson heating, which follows J changing sign. Depending on whether the temperature in a material is directly or inversely related to the generated potential from the charge carriers moving from the hot side to the cold side, heat will be emitted or absorbed, respectively. By measuring the Thomson Coefficient versus temperature, a material's Peltier and Seebeck Coefficients can be determined without needing a junction with a secondary material. The measured material could then be used as a reference material in a thermocouple junction with other materials to determine the secondary material's coefficients as well.

2.1.4. Thermoelectric Figure-of-Merit

The efficiency of a thermoelectric device is dependent on a combination of materials parameters which together comprise the material figure of merit ZT. The figure-of-merit (Z) is a quantity used to indicate the thermoelectric efficiency of a material. The figure of merit of a material is defined as:

$$Z = \frac{S^2 \sigma}{\kappa}$$

where S is the Seebeck Coefficient, σ is the electrical conductivity, and κ is the thermal conductivity. By multiplying Z by the ambient temperature, T, ZT becomes a

unit-less number that increases as the thermoelectric performance of a material is improved. A high Seebeck Coefficient, or thermopower, is necessary for maximum conversion of heat into electrical power. A high electrical conductivity is also important for increased electrical conduction and for reduced Joule Heating, which occurs because of finite resistivity of the material, resulting in conduction electrons losing energy gained from the electric field to phonons. Thermal conductivity must be minimized so the material acts as a thermal insulation between the hot and cold sides, thus maintaining a larger temperature gradient across the conductor, which in turn generates a greater Seebeck Voltage. The power generation efficiency will reach the Carnot Limit as ZT increases toward infinity.

Many difficulties arise when designing thermoelectric materials because of the complex relationships between the material parameters themselves. Thermopower and electrical conductivity have inverse dependencies; improving one may result in decreasing the other, while minimizing thermal conductivity may result in decreased electrical conductivity through the Wiedemann–Franz law, which directly relates the two conductivities for a metal. However, the Wiedemann–Franz law assumes that the both electrical and thermal conductivity are due to the same carrier (electrons). In a semiconductor, the thermal conductivity has an electrical and lattice component, corresponding to the electron and phonon contributions. The relative contributions will change with temperature and with carrier concentration, creating an additional level of complexity for material designers. Figure 2.2 below shows the optimization of various material parameters for Bi_2Te_3 through carrier concentration tuning. The

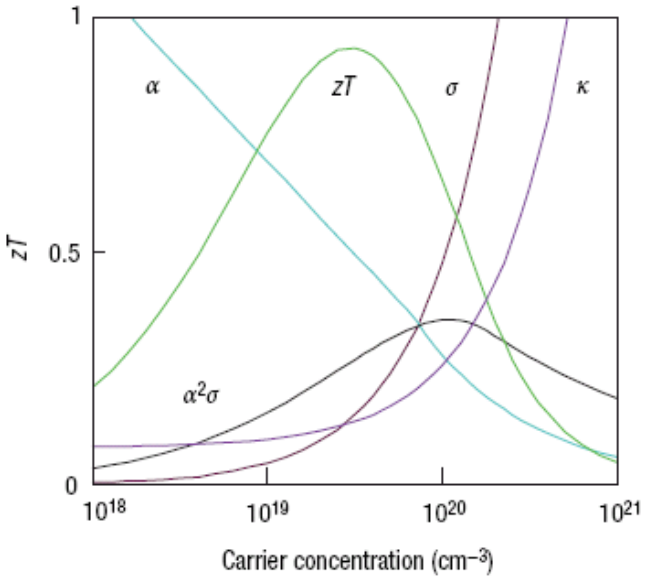

Figure 2.2: ZT versus carrier concentration for a BiTE module.

curve for ZT has a maximum at a different carrier concentration than the maximum power factor concentration, showing the necessity for a compromise between all the parameters.

While there have been many reported materials with ZT > 1.5 at room temperature, these high values are not reproducible by other research groups, nor are devices ever fabricated that demonstrate such efficiency. Bi_2Te_3 is considered a state-of-the-art material, but only demonstrates a peak ZT of 1.1, with an effective ZT of 0.7 overall when used as a cooler or power generator. In order for thermoelectric materials to be economically competitive with mechanical electricity generation methods, an average ZT greater than 3 will be necessary.

2.1.5. Thermoelectric module

A thermoelectric module usually consists of many thermo-elements, alternating n- and p-type semiconductors, joined electrically in series by contacts that are thermally and electrically conductive. The thermo-elements are also connected thermally in parallel by thermal conductors that are electrically isolated. This structure is designed to get an increased voltage produced across the module by having the elements in series, while maintaining temperature uniformity across the module surface. Typical materials used for the contacts and thermal pathways are copper and aluminum oxide, respectively. Layers of ceramic are usually placed on each side of the module and adhered to the module with thermally conductive paste. Since the ceramic wafers have a high thermal conductivity, but are electrically isolated, the current will not short before travelling through the whole series of elements, and will create good thermal contact between the module and the surface to be heated or cooled. A typical thermoelectric module is shown below, with a schematic view of a single pair of the thermo-elements for additional details.

Figures 2.3 and 2.4 below show the schematics for a typical module, which contain alternating N- and p-type "legs" that are connected electrically in series. If one side of the module is heated, the charge carriers (electrons in the N- type and holes in the P-type material) will move to the opposite surface, transporting heat away from the hot side of the module. This will cause electrons to move in one direction through the elements in series, creating a current in the appropriate direction. When the module is used in this configuration, it's useful to have a heat sink on the cold

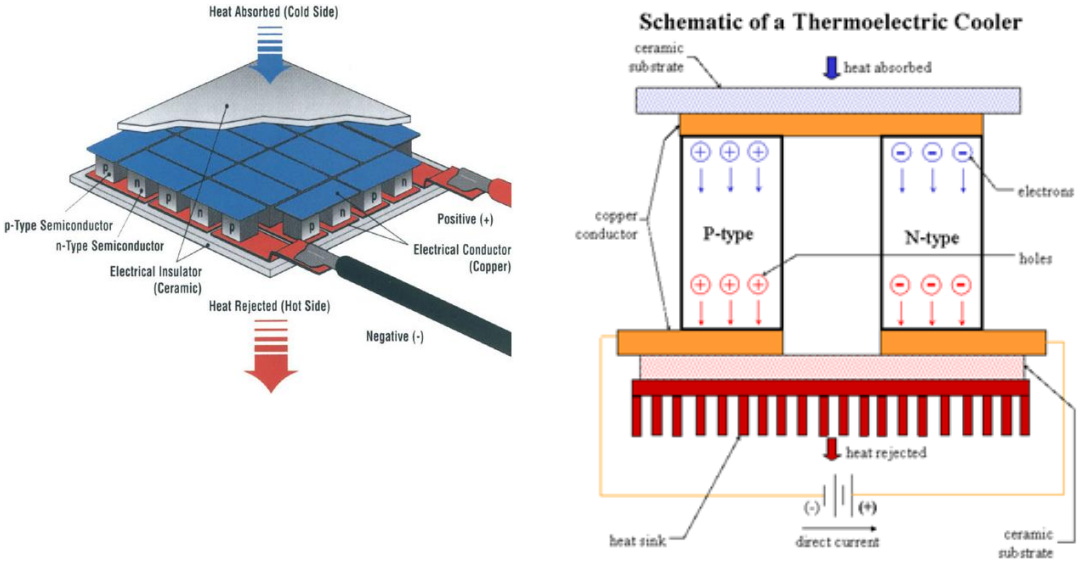

Figure 2.3 and 2.4: Schematic diagrams showing the design of thermoelectric modules.

side of the module for heat dissipation to maximize the generated current. Inversely, if current runs through the device, the module behaves as a heat pump, raising the temperature on the side where the carriers move to, while cooling the other side. The surfaces of the module will be heated or cooled appropriately, based on the direction of current.

2.2. Solar Concentration

Concentrated solar power**,** or CSP, systems position mirrors and/or lenses to concentrate a large area of sunlight onto a smaller area. Typically, some kind of receiver is placed at the focal point of the concentrator, such as a solar cell or fluid

reservoir. Electrical and/or thermal power is produced when the concentrated light is used by the receiver. For the fluid reservoir, the collected heat would be used to drive a heat engine, such as a steam turbine or sterling engine connected to an electrical generator.

2.2.1. Solar Potential

To fully understand the energy potential of solar power, it is useful to see how much energy is incident on the Earth from the sun each year. During peak exposure, the sun produces approximately 100 watts of power per square foot on the Earth's surface. Assuming 12 hours of sunlight per day, and knowing there is 365 days in a year, it can be calculated to show that 438 kilowatt-hours of energy are incident on the Earth per square foot per year. Additionally, there are 27,878,400 square feet per square mile, translating to 12.2 billion kilowatt-hours of energy from the sun per square mile per year. The total surface area of the Earth, including water and land, is 197 million square miles, meaning that 2.4×10^{18} kilowatt-hours of energy are incident on the Earth from the sun per year. If this quantity is converted into quads of energy (8×10^{15} kilowatt-hours per quad), we see that 8.2 million quads of energy hit the earth every year. Human civilization uses approximately 400 quads of energy annually, which means the sun sends 20,000 times more energy to the Earth than humans use annually. Since the above calculation assumed peak exposure, divide the value in half, and there is still 10,000 times more energy than humans use annually. If a system efficiency of 20% can be achieved, we would only have to collect the incident

energy of 1/2000 of the Earth's surface, or 100,000 square miles, which is the equivalent land area of the state of Oregon. In other words, if we were able to collect and distribute all of the solar energy incident on the state of Oregon for an entire year, we would have enough solar energy to provide all of humanity's energy needs for that year. While this statement sounds simple, it is also important to consider energy storage, distribution, system maintenance, funding, and infrastructure changes to accommodate the system. Nevertheless, there is a great deal of available energy that should be utilized.

2.2.2. Solar Thermal Versus Photovoltaic

There are several key differences between photovoltaic and solar thermal technology. In the case of photovoltaics, or solar cells, the light from the sun is directly converted into electricity. This energy can only be efficiently collected and used during daylight hours, since electricity storage is rather inefficient. Therefore, continuous energy availability is lacking with photovoltaic technology. On the other hand, solar thermal systems concentrate solar irradiation to generate heat, which is used to run a heat engine that produces electricity from the heat. The thermal energy from the sun is typically used to heat some kind of fluid, such as water or molten salt, which is stored within an insulated container. Different types of engines can use the stored heat to generate electricity, such as steam engines or gas turbines. Typical engines can produce 100's of megawatts of power, with efficiencies on the order of 30-40%. After the sun goes down, the thermal energy that was accumulated over the

day continues to generate electricity. Since heat storage is more efficient than electricity storage, solar thermal becomes a much more attractive technology over photovoltaic systems for large-scale implementation.

There are two forms of solar thermal collection: line focus and point focus. Line focus uses a parabolic mirror to concentrate light which rotates to follow the sun during the day. Point focus uses an array of mirrors that all focus light toward a central power tower. Line focus is less expensive and less technical than point focus, but the achieved efficiencies of point focus is much greater. Line focus solar thermal plants are reporting concentrations around 80-100x. However, greater concentrations are difficult to achieve, due to errors in thermal expansion, shifting of hardware with time, and optical misalignment of various parts. At these concentrations, a steam turbine achieves roughly 25% efficiency. Point focus requires a larger land area for all the mirrors, but can achieve substantially higher temperatures, and therefore, much higher efficiency. Point focus technology is reaching ~1,000x concentration. This concentration ratio can run a steam turbine at 35-50% efficiency, with plenty of room for improvement. With all things considered, point focus systems are more expensive, but typically achieve a greater kWh/cost than line focus.

Another significant challenge for solar thermal energy generation is the amount of space required for efficient energy production. Solar thermal plants, such as the one in Burbank, CA, shown in Figure 2.5 below, need at least 1/4 to 1 square mile of land to install a sufficient number of mirrors to achieve the concentrations

Figure 2.5: An eSolar solar thermal system in Burbank, California.

previously discussed. Additionally, the land used needs to receive a consistent quantity of direct sunlight. Deserts and other arid landscapes are ideal locations for solar thermal plants to establish themselves and flourish, due to plentiful amounts of sunlight. Additionally, many solar thermal companies are investigating areas previously ideal for agriculture. As farmland is overused or damaged due to human activity, that land can still be useful for energy production. It would require a substantial amount of land usage to install enough solar thermal plants to be able to provide a significant portion of the country's energy demand.

2.3. Thermal and Electrical Cogeneration

One of the major advantages that thermoelectrics offer is that they are solid state devices, which means they have no mechanically working/moving parts. This attribute enables thermoelectric devices to have none of the maintenance

requirements normally associated with mechanical devices, in addition to having a much greater lifespan. In the case of conventional solar thermal systems, a sterling engine or steam turbine is typically used to generate power from the heated fluid. These systems have maintenance needs, such as lubrication and replacing worn parts. Additionally, thermoelectrics work exceptionally well when large temperature differences exist. In the case of solar thermal systems, the central receiver temperature will get as high as 1000 K, depending on the size of the system and the fluid used in the receiver.

To determine the hot side temperature of the thermoelectric material as heated by the concentrated solar radiation, the thermal resistance and incident radiation must be calculated. For determining the incident radiation on the receiver, it is important to consider the Earth's solar constant for your location and day. With the sun directly overhead, which occurs at the equator at high noon, the solar constant of the Earth is 1.37 kW/m^2. Since the sun is rarely overhead, additional considerations should be taken to determine the exact location of the sun. First, the Earth will tilt according to the time of year. Over the whole year, the Earth experiences a maximum tilt of 23.5 degrees. The Earth has no tilt around March 21st and September 21st. We can thus make an estimate for the suns position north of the equator, θ, with the following equation:

$$\theta = 23.5° \sin(2\{T/365.25\})$$

where T is the number of days compared to April 21st, the vernal equinox. If we know our latitude, L (Santa Cruz is located at 36.97 N), we can get an estimate for the solar constant on a given day for our location by:

$$\sigma = (137\text{mW/cm2}) \cos (\text{L} - \theta)$$

In the case of the presented measurements, all were performed in August, which means that the solar constant varied from 1.24 kW/m^2 to 1.27 kW/m^2 over the course of all the measurements. Additional accuracy can be determined using a solar meter to directly measure how much solar energy is incident, but such a device was not available. By knowing the size of the concentrating dish, the energy concentrated onto the receiver can be determined.

After determining the solar constant, I also had to determine the thermal resistance of the receiver. By knowing the thermal resistance, I could estimate how much incident power would be required to attain a given temperature. To determine how much the dish will increase the temperature of the receiver, the following equation was used:

$$\Delta\text{T} = \text{Q} * \text{Rth} = (\text{L/AK}) * \text{Q}$$

where Q is the incident energy on the receiver from the dish, L is the thickness of the receiver, A is the surface area of the receiver, and K is the thermal conductivity of the receiver. As the receiver is a thermal network of different materials in series with one another, the dimensions and thermal conductivity must be considered separately and

then added together. The thermal resistance for the receiver, along with the concentrator dish size will be discussed in the results.

2.4. Optimal Power Output

In 1840, Moritz von Jacobi experimented with optimizing the output power of a battery. A battery can be represented in a circuit as an electromotive force, E, in series with an internal resistance R. If an external load with resistance R' is placed in series with the battery, then the current through the circuit is:

$$I = E / (R + R').$$

The power dissipated in the load is I^2R', while the power dissipated in the battery is I^2R. If R' = 0, there is no external power through the load. If R' = ∞ there is also no power transferred, since I = 0. Therefore, for some intermediate value of R', there must be a maximum power, which will occur when R' = R. Hence, Jacobi's theorem states that maximum power is transferred when the internal source resistance equals the load resistance. However, his theorem results in maximum power transfer, and not maximum efficiency. If the load resistance is greater than the source resistance, then the efficiency is higher, since a higher percentage of the source power is dissipated to the load, but the magnitude of the load power is lower since the total circuit resistance will increase. In the case of my experiment, I was trying to achieve the maximum electrical power output from the thermoelectric module, since the overall system

efficiency will depend on the generated electrical power, in addition to the absorbed thermal energy from the water.

2.5. LabView

LabView is a graphical programming tool developed by National Instruments to simplify the programming process for researchers and engineers. The software has two separate windows for ease of use: a "front panel" where the user interface can be optimized, and a "block diagram," where all of the coding is contained for the program. Figure 2.6 below shows these two windows for the data acquisition software used in this project. This creates two separate environments that can be designed for optimal end-user convenience in conjunction with ideal programmer troubleshooting capabilities. It has all of the typical programming tools found in most mainstream software (for example, Fortran or Matlab), such as Boolean logic, sequencing and mathematical functions, except all the programming is represented as graphical icons and wires that resemble a flow chart. Each function in the code has a graphical node with inputs and outputs. As soon as the flowchart feeds all the inputs to a given node, that node can complete its process and produce all of its outputs. This gives the programmer the ability to execute multiple functions in parallel. The graphical format also greatly simplifies the troubleshooting process by displaying where errors occur in the code. LabView has a feature that can be toggled on that slowly executes the code, showing the user where the code is in its execution. If an error occurs along the way, it will notify the user as the code is running and direct them to the source of the

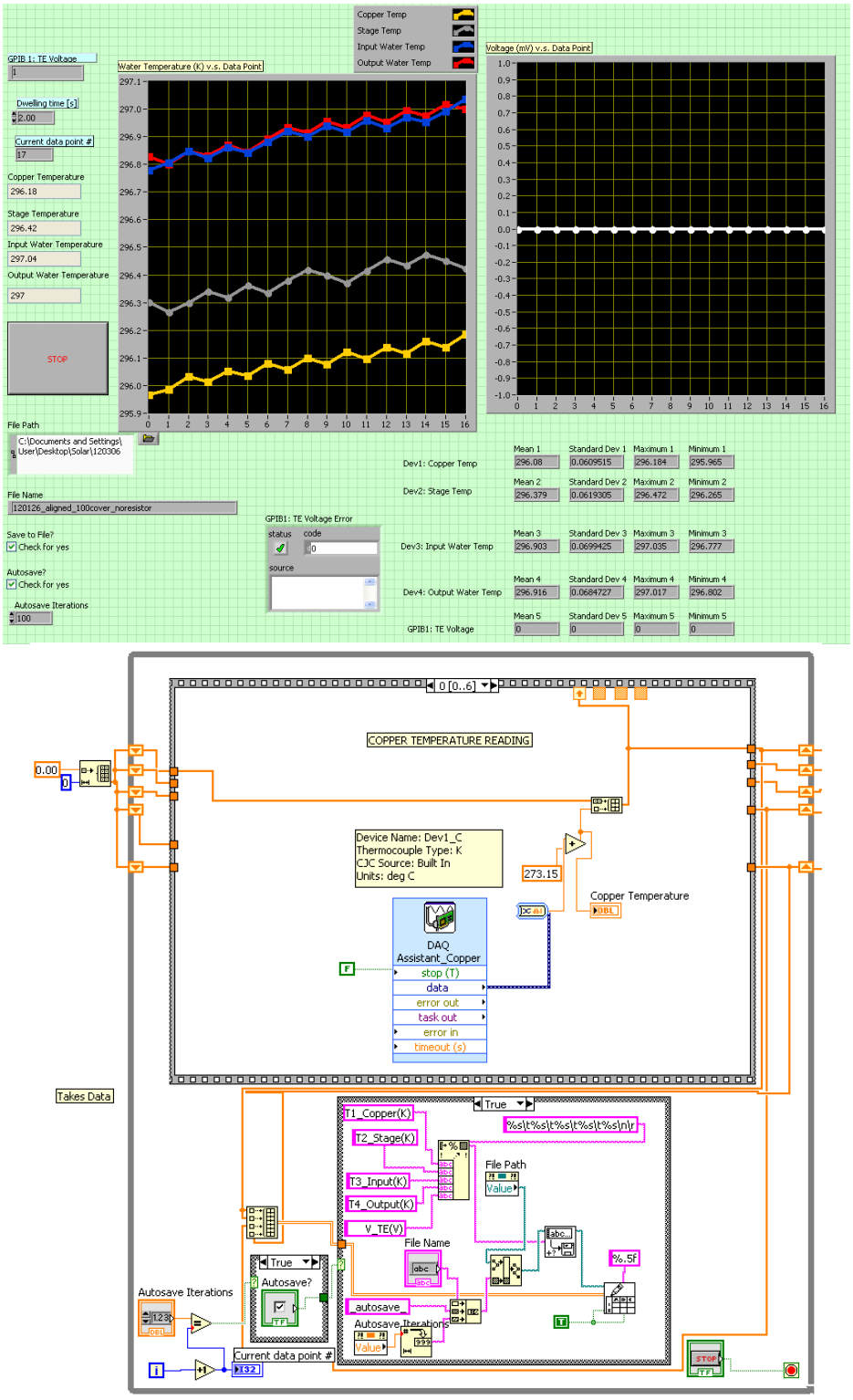

Figure 2.6: Front panel and section of block diagram for the measurement program.

error, with a suggestion as to the likely reason for the error code. LabView also has many convenient features relating to hardware interfacing, such as VISA and GPIB communication. This enables the programmer to build and automate very sophisticated measurement tests and control systems that use external hardware. Many hardware manufacturers, such as Keithley Instruments, which developed the 2400 Sourcemeter used in this project, collaborate with National Instruments to develop drivers for their instruments that are used directly by LabView. LabView can also record any collected data in various file formats, such as spreadsheets or images, making data analysis much simpler.

2.6.ANSYS

ANSYS Inc. is an engineering simulation software developer that offers a comprehensive range of simulations, providing access to virtually any field of engineering simulation that a design process requires. Companies in a wide variety of industries use ANSYS software. The tools are designed to put a virtual product through a rigorous testing procedure before it becomes a physical object. For the thermal simulations, we have used ANSYS Mechanical APDL, which stands for ANSYS Parametric Design Language, a scripting language that you can use to automate common tasks or even build your model in terms of parameters (variables). While all ANSYS commands can be used as part of the scripting language, the APDL commands discussed here are the true scripting commands and encompass a wide

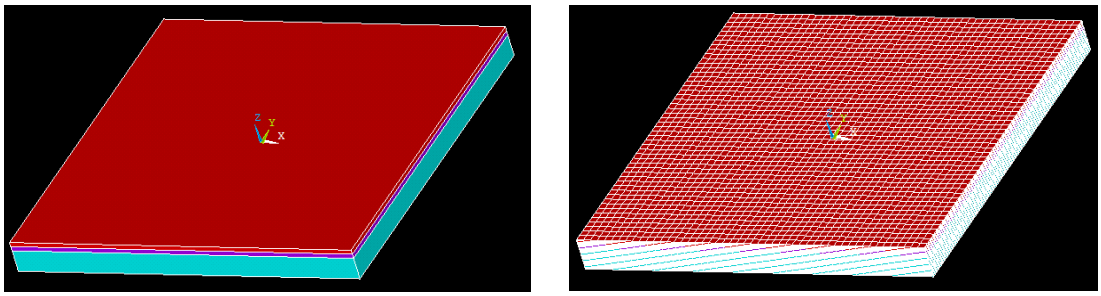

Figure 2.7. Built model of the TEM, along with the meshed structure. The red volume is the copper layer, the purple is the insulating layer and light blue is the TE material.

range of other features such as repeating commands, macros, if-then-else branching, do-loops, and scalar, vector, and matrix operation. While APDL is the foundation for sophisticated features such as design optimization and adaptive meshing, it also offers many conveniences that you can use in your day-to-day analyses. The ANSYS program has many finite-element analysis capabilities, ranging from a simple, linear, static analysis to a complex, nonlinear, transient dynamic analysis. Specific procedures for performing analyses for different engineering disciplines are described in ANSYS software powerful help.

The process for a typical ANSYS analysis involves three general tasks: building the model, applying loads and obtaining the solution, and reviewing the results. These steps include choosing parameters, units, meshing the structure, applying loads and boundary conditions, choosing the right solve, etc. For our thermal simulations, we used 20 solid elements. The structure of the TEM is built and meshed, as shown above in Figure 2.7. Several simulations were run to make sure

that the meshing is correct and the results converge while operating under appropriate loads and boundary conditions. Then, we applied the boundary conditions and loads. A constant temperature of 300 K was set for the bottom layer and several different heat flux maps were applied for different simulations on the top layer. The rest of the areas boundary conditions were set automatically to adiabatic. A sparse solver is chosen to perform the analyses and solve the appropriate equations to find the temperature in different nodes and elements. These simulations were used to evaluate how to improve the system to avoid overheating and to ensure a uniform temperature profile on the receiver.

3. Experimental System

The system developed for this project has several sections that will be described. I will explain the function of each section, in addition to any theory that was considered when deciding on various parameters. The experimental system can be divided into the following sections: the tracking system, the receiver, the cooling system, and the measurement system. Figure 3.1 below shows the various components of the setup. The tracking system was designed and built with significant help from the Jack Baskin School of Engineering Machine Shop at University of California, Santa Cruz.

3.1. Tracking System

The solar tracker is designed to support the concentrator and the receiver, in addition to being able to follow the sun as it travels through the sky. The tracking system has several core sections, including the parabolic mirror, the tracking frame, and the tracking circuits.

3.1.1. Parabolic Mirror

The parabolic mirror is a dish that collects the incident sunlight and concentrates the irradiation to a focal point. A receiver system is placed at the focal point of the mirror to produce power from the incident energy. The size of the dish will determine the power input of the collection system. Two sizes of dishes were used in this project: a 35” diameter dish and a 25” diameter dish. Originally, the 35” dish was used for the

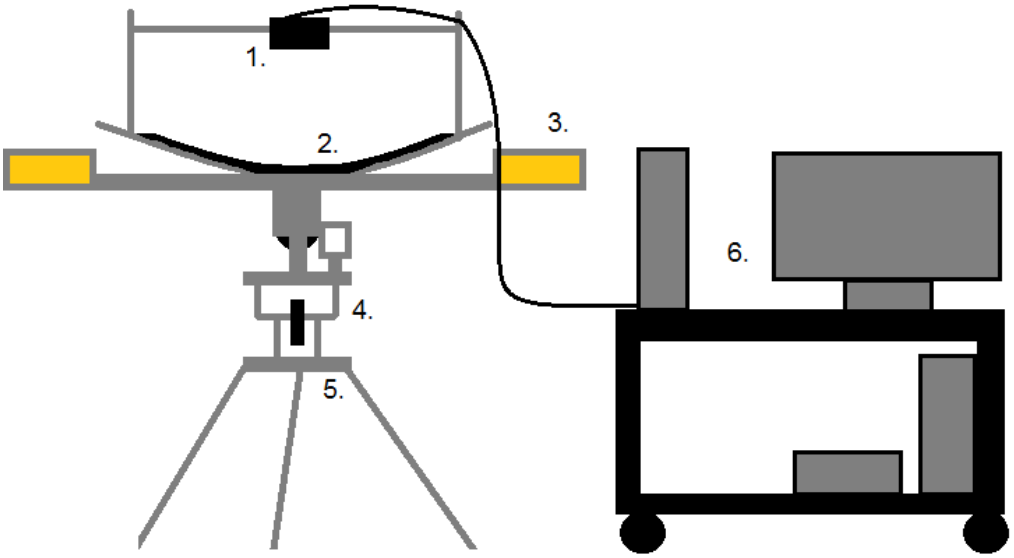

Figure 3.1: Solar tracking system: 1. Receiver and cooling system. 2. Parabolic mirror 3. Tracking circuit. 4. Tracking plates. 5. Support tripod. 6. Measurement system.

experiment, but after some calculations and some measurements, the dish collected too much incident energy and would overheat the receiver. A majority of the receiver components, such as the cooling hoses and delrin sample mounting clamps, are not rated to survive temperatures beyond 550K. However, upon calculation using the incident power of the dish and the thermal resistance of the receiver, the expected hot side temperature of the thermal receiver was on the order of 600K. While the larger dish was still mounted, measurements were performed by covering half the dish with a bed sheet to prevent the incident radiation from reflecting onto the receiver. Later, a 25” dish was used for comparison with the 35” dish. The concentration ratio of the 25” dish is 82x, approximately half of the 35” dish concentration ratio of 162x. The

Figure 3.2: Image of the tracking frame

expected heating of the sample was expected to be around 175 K above ambient temperature, which was within threshold temperatures of most components.

3.1.2. Tracking Frame

The solar tracking frame used in this experiment was designed to optimize the performance of the solar collector. The main components of the tracking frame include a support tripod, two tracking platforms for the mechanical tracking system, and a support frame which secures the tracking circuits, the parabolic mirror, and two support arms for the solar receiver. These features allow the user to efficiently and

precisely control many aspects of the collection setup. Figure 3.2 is a picture of the solar tracking frame shown above.

The base of the tracking frame is secured to a tripod. This tripod has a panel on top that can rotate 360 degrees to allow the frame to be manually rotated to align with the sun. This enables the user to make quick adjustments as needed. The legs of the tripod are attached to the base by a ball joint, enabling the leg to be rotated in all directions. Each tripod leg also has an adjustable length to vary the height of the frame above the ground and for leveling the tripod on uneven surfaces. These two attributes enable the user to level and balance the frame to provide optimal support for the setup, preventing wind or torque from the dish weight from causing the dish to fall over. After the legs have been moved to the desired position, there are screws that can be tightened to hold the leg settings in place. As a failsafe to the screws holding the legs in place, a strap is additionally placed around the legs at a fixed length to ensure that no abrupt shifts in the tripod legs occur.

There are two tracking plates that connect the dish support to the tripod, shown below in Figure 3.3. The tracking plates possess several features to optimize their mechanical performance, including, the AC-DC power converters boxes, the motor box and gear reduction, and the limit switches. The white plastic boxes, seen on the top plate, contain AC-DC power converters that supply power to the tracking circuits. This conveniently allows the user to plug in a conventional AC plug into a socket, and power the tracking circuit with the 12 V DC source it requires. This

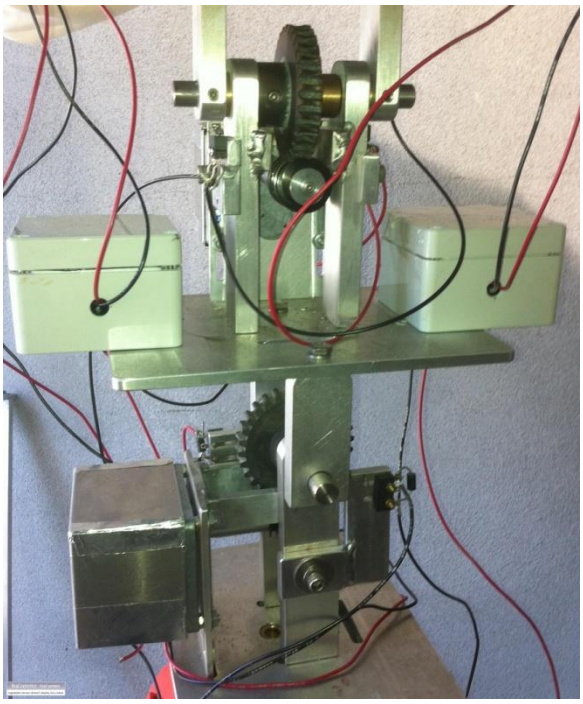

Figure 3.3: Image of the dish alignment platforms with mounted protective boxes for the motors (metal) and power converters (white). The wires connect the motors and power converters to the tracking circuits.

bypasses the need for extra instruments, such as a DC power supply. The tracking circuits have wires that feed down to the metal boxes, which serve as weatherproofing to protect the mechanical motors that adjust the axes of the dish. Holes were placed on the bottom of the cover to allow wire access without exposing the motors to the weather. The motor inside the metal box is connected to the black gear cylinder, which rotates when the tracking circuit sends it a signal, which in turn, rotates the large gear controlling the tracking axis. The large gear is used for gear reduction, which prevents the high rotational speed of the motor from rotating the frame too quickly. This allows the circuit to make subtle changes in the frames position for

more precise alignment. Finally, each plate has a pair of limit switches mounted on key structural locations along the direction of tracking. If the motor rotates the tracking plate too far along one axis, the frame will move against the limit switch, triggering a relay to break the current path, thus preventing the frame from moving further in that direction. This prevents the system from damaging itself from rotating too far. Each tracking plate controls a different degree of freedom. Originally, the two desired axes of control were supposed to be North-South and East-West. However, due to an incorrect design, the bottom plate controls the azimuthal angle of the frame, which is not useful, and the top plate controls the North-South alignment. Due to assembly time limitations, the frame was not modified to correct this, however an alternative design for the bottom plate was developed that would correct the issue, as shown below in Figure 3.4. Due to this design flaw, alignment adjustments for the horizontal direction were made manually by rotating the frame on the tripod's base.

The support base possesses an X shaped base to secure the parabolic mirror, a pair of arms for mounting the tracking circuits, and two clamps for securing the receiver support arms to the frame. The mirror base has four arms in the shape of an X that bend up parabolically to match the curvature of the parabolic mirror. This base is designed to hold the mirror in a natural position for focusing light onto the receiver. To secure the mirror to the base, a plastic-to-stainless steel epoxy was applied to the steel base and the mirror was placed on top. Pressure was carefully applied to ensure the epoxy had good contact with both the base and the mirror. The mirror used for this project has an acrylic (plastic) protective coating on the back side. The support

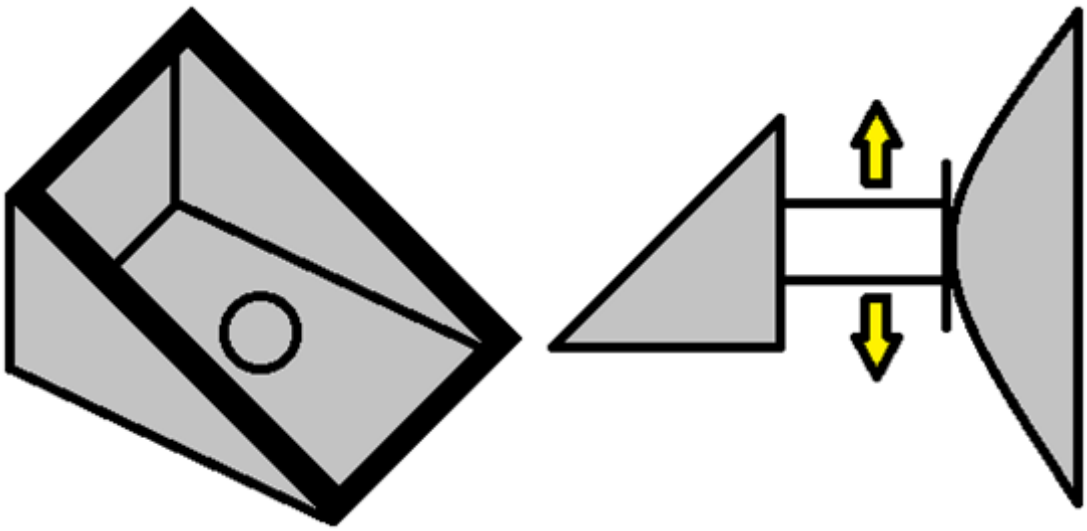

Figure 3.4: Alternate tracking plate design for fixing tracked axis. Current design adjusts incorrectly when one plate is at maximum adjustment from center.

base also has two steel arms that extend out past the diameter of the mirror to hold the tracking circuits. This design was used to ensure the tracking circuits' shadow blocks were along the same axis with respect to the center of the mirror. This would guarantee that the focal point of the mirror would be adjusted appropriately as the tracking system aligned itself with the sun. Finally, the support base has two clamps that secure the receiver arms to the support base. These arms are used to secure the receiver at the desired location with respect to the focal point. The receiver system mounts onto a cross beam that has each end secured to the support arms via bolts. The support arms have long channels cut into the arms so that the user can adjust the receivers distance from the center of the mirror. The receiver also screws onto the support beam in a way that it can be slid along the beam for additional positioning

accuracy. These adjustable features allow the user to precisely control the position of the receiver with respect to the dish to optimize the incident energy arriving at the receiver surface.

3.1.3. Tracking Circuits

An important aspect of a solar energy system is the alignment of the solar receiver with respect to the sun. As the day progresses, the sun moves across the sky in a simple arc. The parabolic mirror needs to be aligned with the sun to maximize the amount of incident energy that is subsequently focused onto the thermoelectric module. If the system is not aligned correctly, the location of the focused light will shift partially or completely away from the receiver. This misalignment will make it impossible to determine the incident energy on the receiver for the purpose of calculation, in addition to an actual decrease in the hot side temperature of the thermoelectric, leading to a reduction of the electrical power generated. To ensure that the system alignment is optimized, sun tracking circuits were assembled and installed on the frame to continuously correct the alignment of the system. The tracking circuit diagram is shown below in Figure 3.5. The two features that these circuits must include are the ability to sense where the sun is presently located, and it needs to be able to move itself to be realigned with the sun. To sense and align with the sun's location, the project utilizes a feedback control system, consisting of a pair of photocells divided by a piece of material, referred to as a "shadow block," shown below in Figure 3.6. Each photocell is connected in series with a 1 kOhm resistor to

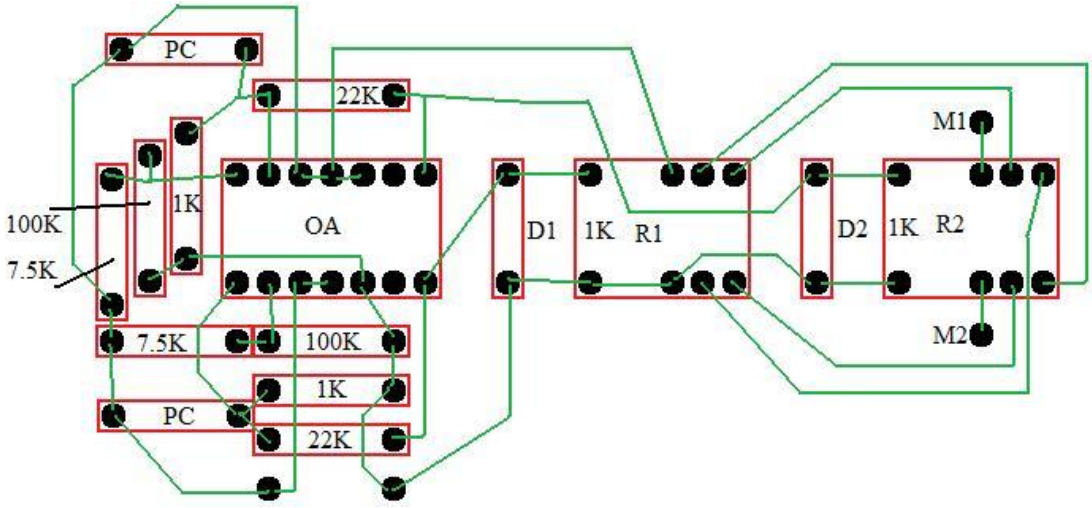

Figure 3.5: Schematic of the sun tracking circuit. The circuit was built from a kit purchased from MTM Scientific.

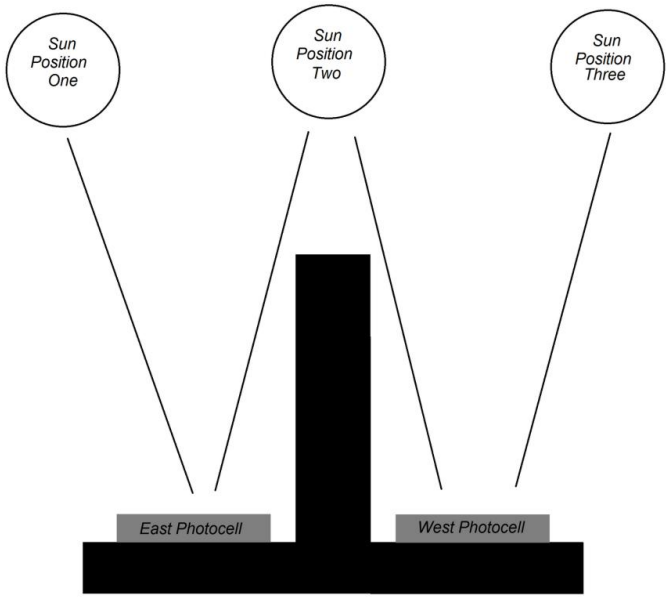

Figure 3.6: Feedback control system using two photocells separated by a shadow block.

form a voltage divider. The “trigger point” of the circuit is determined by comparing the photocell voltage divider with another fixed voltage divider. An IC comparator then senses the voltages from the dividers to then trip an appropriate relay. The sensitivity of the trigger point of the relays can be adjusted by changing the resistors used in the fixed voltage divider. If the sun is in position one, the shadow block will cast a shadow across the West photocell. This will increase the resistance of the shadowed photocell, thus reducing the voltage across the voltage divider. This change in the comparator voltage is then used to trigger relays that will open and close various paths. In the case where the sun is in position one, the relays will connect a path that will send power to a motor that will adjust the position of the circuit until it is correctly aligned to position two. Once the system is aligned to position two, both photocells receive equal incident energy, which will set the relays to have an open path, thus preventing the motor from receiving power for further adjustment. Similarly, as the sun moves to position three, the relays will respond to create a path that sends current in the opposite direction through the motor, making it run in the inverse direction to realign the sun back to position two. By mounting the circuit on the same axis of rotation with the dish, the circuit will always be aligned with the sun as the motor rotates the system, which will in turn be aligned with the dish. The alignment sensitivity of the circuit can be controlled by the height of the shadow block. By having a taller shadow block, or by having the photocell closer to the shadow block, the tracking circuit will be more sensitive, with a smaller misalignment resulting in a shadow being cast over a photocell, which will result in an adjustment.

Problems may arise in this circuit when the voltage from the photocell is very close to the trigger point. When this state exists, the relays that are controlled by the comparator may switch on and off erratically as the voltage fluctuates around the trigger point. By providing positive feedback with an additional resistor at the output of each operational amplifier, we can introduce damping called hysteresis to the circuit to prevent this undesirable behavior.

After the circuit was assembled, it was mounted in a "weather-proof" enclosure. The enclosure was a plastic container with a transparent plastic lid to allow the circuit to still trigger from the sun. Sealants were used at the interface between the container and lid to prevent moisture from entering the enclosure. Holes were drilled into the plastic enclosure for mounting onto the frame, and so that wires could leave the enclosure and reach the motors attached to the frame. These holes were then water-sealed using silicone.

Automated devices with mechanical limitations should include limit switches to prevent damage to the system. Figure 3.7 below shows a circuit diagram with limit switches, which are used to open the current path if the switch is actuated. For the purposes of this system, the limit switches are mounted in mechanical locations that will restrict the operational range of motion for the tracking system. For example, if the dish motion were not restricted, it could rotate too far and push against the tripod support, causing the dish to be broken off of the frame if given enough time. With the limit switches mounted near the rotating axis of the dish, the limit switch will be

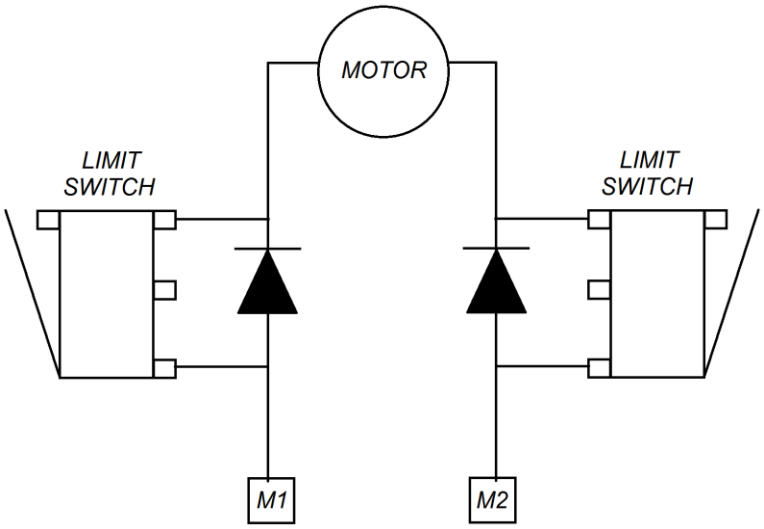

Figure 3.7: Circuit diagram using limit switches for controlling motor motion range. The limit switches prevent the motors from moving the frame into a position that would cause damage, while the diodes enable the motor to be reversed if a switch is triggered.

tripped by the frame before motor or frame damage is done. By including the limit switches in the current path to the motors, the motor will be disabled when it moves the frame in a way that trips a limit switch. Normally, the tracker would require a manual reset after tripping a limit switch. However, by running the limit switch in parallel with a diode, the frame will be able to rotate away from the limit switch by using the diode path. This enables the system to be easily reset at the end of the day or the beginning of the next day.

Originally, this circuit was designed to operate using a DC power supply. However, for the sake of convenience, AC-DC power converters were installed to simplify the process for powering the tracking circuits. Now, the circuit can be

powered by simply plugging the circuit into an outlet. This minimizes the number of devices needed for the experiment. However, a power study needs to be done to evaluate the benefit of aligning the system. If the power used to track the sun exceeds the additional power the concentrator generates by being more aligned, there is no incentive to have such precise tracking. To determine the power required by the tracking circuits, I examined the voltage needed by the circuit (12 V), in addition to the circuit resistance, which was around 1 kOhm. Ohm's Law can be used to determine the needed power:

$$Power = \frac{V^2}{R} = \frac{(12\ V)^2}{(1000\ Ohm)} = 0.144\ Watts$$

As there are two tracking circuits, the total power required to run the tracking system is 0.288 watts. This power need should be insubstantial compared to the output of the thermoelectric module used.

3.2. Solar Receiver System

The solar receiver is positioned near the focal point of the parabolic mirror to use the collected solar energy. The diagram below shows a cross section of the receiver. There are several material layers that combine to become the receiver, including a copper heat spreader, two ceramic wafers, the HZ 14 thermoelectric module, delrin clamps, the water cooled aluminum heat sink and the tubing for the water pump. Many of these items came as a kit from a company called Hi-Z

Technologies. The thermoelectric module generates electrical power from a temperature gradient. The hot side will be established by the incident solar energy from the parabolic mirror, and the cold side temperature is controlled by the water cooling system. The ceramic wafers are adhered to each side of the thermoelectric module using thermal grease. The ceramic is thermally conductive but electrically isolated to prevent the module from electrically shorting while still creating good thermal contacts on each side of the module. Additional thermal grease is then used to sandwich the module between the copper heat spreader and the water cooled aluminum heat sink. The copper heat spreader is used as a top surface for the receiver system and will be directly heated by the incident energy. Since copper has a very low specific heat capacity, or the amount of energy required to raise the temperature of a given material, the copper heat spreader can quickly distribute the incident energy to create a uniform hot side temperature across the active area of the thermoelectric. This temperature uniformity is important for optimizing the overall efficiency of the module. If the temperature distribution is not uniform, the voltage across each leg in the module will be decreased in various spots, resulting in an overall decrease in the produced voltage for a given temperature difference. Two separate copper heat spreaders were used in the experiment: one normal copper plate and one

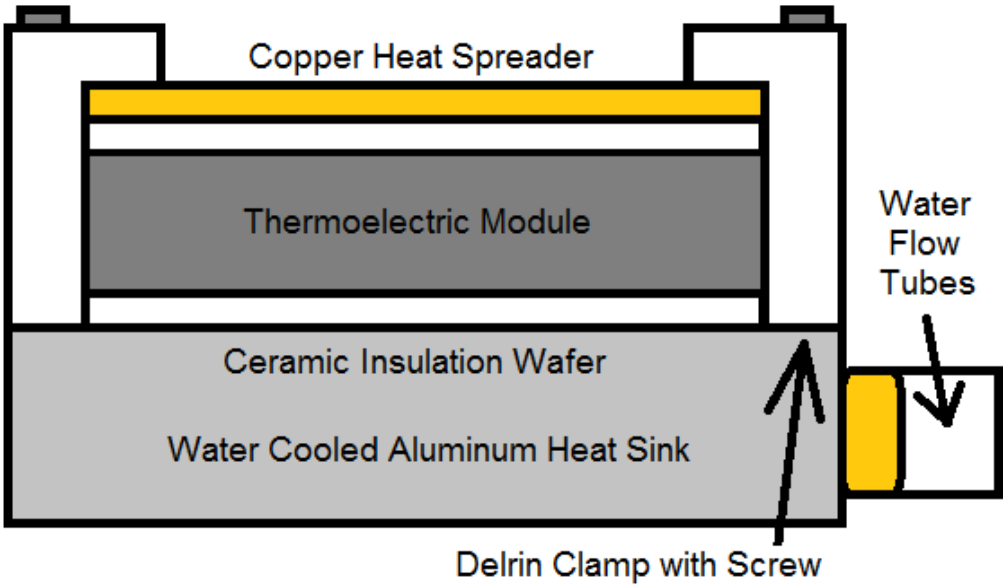

Figure 3.8: Cross section of solar-thermal receiver.

copper plate spray-painted black. The black copper plate will have a greater absorption of the incident energy and therefore the receiver should operate at a greater temperature difference.

3.3.Water Cooling System

The water cooled aluminum heat sink is used to establish the cold side of the module. Like copper, aluminum also has a low heat capacity, but by being in thermal contact with cold water, which has a high heat capacity, the heat sink can be held at a lower temperature to maintain the large temperature gradient across the module. The heat sink has a serpentine path inside to maximize the interface surface between the water and the aluminum for extracting as much heat from the system as possible. The flow rate of the water will determine the cooling power of the heat sink. By having a

higher flow rate, the water will take heat away from the system more quickly, resulting in a lower cold side temperature. The water is pumped by a Zalman cooling tower, which is designed for cooling a high performance computer. The tower has a series of thin metal fins stretching out from the tower. This design maximizes the surface to volume ratio, allowing more surface area with which to radiate heat away. The water is pumped through a series of plastic tubing that interfaces with the heat sink via a brass fitting at the input and output. A flow meter is placed within the tubing path, which contains a rotating turbine that calculates the flow rate of the water in milliliters per minute. Without any restrictions on the cooling system, the water is pumped at a rate of 450 ml/min. The flow rate can be reduced by using a clamp to pinch the tube at certain locations to restrict the water flow. Reducing the flow rate will allow the water to absorb more heat energy as it passes through the heat sink, which is desirable if the system is to be used for the cogeneration of hot water in addition to electrical power. However, by restricting the flow rate, the temperature difference between hot side and cold side will also increase, therefore reducing the electrical output of the TE module. In addition, the performance of the cooling system was evaluated when the water was continuously circulated in a closed system, compared to when the water is transferred from a cold reservoir to a hot reservoir.

3.4. Measurement System

The measurement system can be separated into a few components: the thermocouples, the sourcemeter, and the data acquisition software. The

thermocouples are used to acquire temperature information from the receiver, while the sourcemeter is used to measure the voltage output of the TE module. The data acquisition software is then used to record the data collected.

3.4.1. Thermocouples

A thermocouple is a junction of two dissimilar conductors (typically metal alloys) that will produce an electrical potential related to the temperature of the junction. Each combination of materials has a specific voltage response with temperature. The type of materials used for a thermocouple should be chosen based on the temperature range of interest as well as voltage resolution. The thermocouple should also be chosen based on the size of the active area of the device. A smaller thermocouple will be able to measure much smaller active regions and will respond to temperature changes faster, since it will have a lower thermal mass. However, the drawback to using a smaller thermocouple is that the junction will be more delicate and may break easier. Other considerations, such as magnetism or resistance to corrosion, may also be used to determine what materials should be used. In the case of this system, type E thermocouples from Omega Engineering are used, which are made of Chromega-Constantan (Chromium-Nickel Alloy and Copper-Nickel Alloy), and have a Seebeck coefficient of approximately 80 uV/K.

In order to acquire accurate data from the thermocouples, the thermocouples need to be in good thermal contact with the device, which can be achieved using thermal paste. Thermal paste is an electrically isolated, thermally conductive paste

that is somewhat adhesive. These qualities makes thermal paste ideal for achieving optimal thermal flow between the thermocouple and the active device, as well as keeping the thermocouple firmly secured to the region of interest. Since the adhesive quality of thermal paste is reduced as the temperature of the paste increases, this project used thermal paste in addition to mechanical clamping to ensure the thermocouples did not migrate during the measurement.

Many thermocouples have convenient leads for reading the voltage across the junction. National Instruments makes a product called a TC-01 that has a plug for the thermocouple leads and a USB connection for reading into a computer. This device allows the user to read the voltage across the thermocouple junction into LabView using data acquisition software. LabView then converts the voltage into a temperature reading based on what type of thermocouple is used. The temperature readings are then logged versus time and are updated frequently to give the user real time feedback about the temperature of various locations on the solar receiver. For the purpose of various calculations, four thermocouples are positioned on different spots of the receiver to log the temperatures. The locations of interest are the top surface of the copper heat spreader, which tells us the "hot" side temperature of the thermoelectric, the aluminum stage temperature, which tells us the "cold" side temperature of the thermoelectric, and there is a thermocouple mounted on each of the two brass connectors that connect the water hoses to the input and output of the water cooled heat sink. Although the thermocouple junctions are electrically insulated, there was no way to effectively submerge them in the water. Since the water is in constant

contact with the brass fittings, which is a metal with a low specific heat capacity, the temperature of the brass should be close to equilibrium with the water entering and exiting the heat sink. The input and output water temperature needs to be known in order to determine how much thermal energy is being extracted by the water flowing through the system.

3.4.2. Data Acquisition Software

As mentioned previously, software called LabView was used to collect the data for this project. Several devices were used in conjunction with LabView for collecting and recording the data used in this project. A Keithley 2400 Sourcemeter is used to read the voltage across the thermoelectric module, and four National Instruments TC-01 USB Thermocouple Readers are used to read the temperature of four different locations. All of these readings are recorded and plotted versus time as the program runs. The user can control the frequency for which data is acquired by setting the delay between each measurement. The software also displays minimum, maximum and average values for each temperature and the TE voltage. When the program is stopped, it will save the data collected during that run in a spreadsheet, named according to the user's specification, enabling the data to be scrutinized later. The user can also make the program automatically save the data collected after a given iteration is reached to make sure that if something goes wrong before the stop button is pressed, not all the data will be lost. When analyzing the collected data, there is typically a plateau at a given voltage where the thermoelectric is operating at

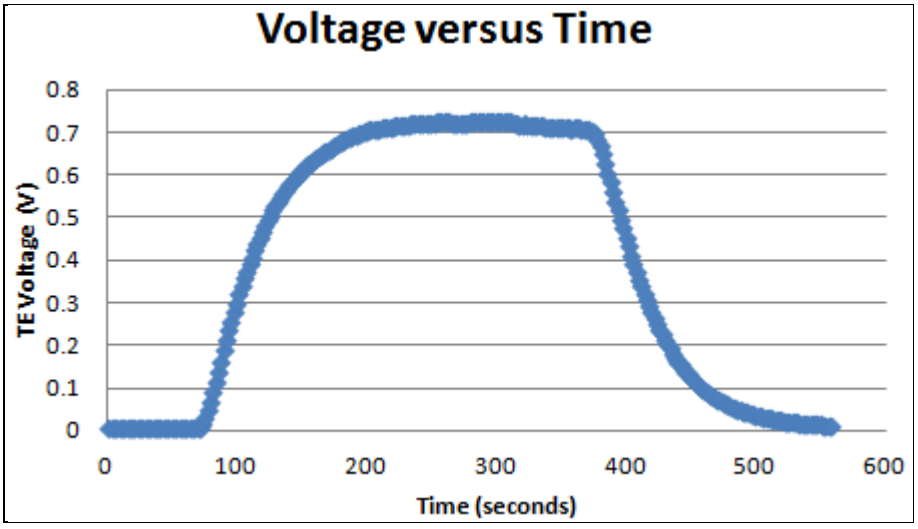

Figure 3.9: Sample graph of the TE module voltage versus time collected by LabView

the maximum temperature it is going to reach, as shown by the sample graph above (Figure 3.9). That maximum voltage is recorded, and then compared with other runs based on the open circuit voltage, or converted into power by considering the load resistance.

4. Results

The following section discusses the results that were gathered from performing a series of experiments using the assembled setup. The objective of these tests was to maximize the overall system efficiency by optimizing the electrical power generated by the thermoelectric module while simultaneously optimizing the thermal energy extracted by the water pumping system. Data was collected using a "first-generation" receiver, and a "second generation" receiver. After data was collected using the first receiver, an ANSYS simulation was performed, based on the results. Using the simulation results, an improved second receiver was assembled and retested. In addition to the receiver improvements, several other tests were performed to evaluate their respective contributions to the system performance. After completing these tests, it is clear that the system has many strengths and weaknesses that will be discussed, in addition to how the weaknesses can be improved if the system were to continue being used for further research.

4.1. First Generation Receiver

The first receiver dimensions used corresponded to what materials were readily available and would be good for preliminary system tests. As discussed earlier, we ordered several items as a kit from a company called Hi-Z Technologies, such as the thermoelectric module, the 0.8 mm thick ceramic layers for each side of the module, and the water cooled heat sink. There was a 0.8 mm thick copper heat spreader with the correct dimensions to cover the module and then the setup was

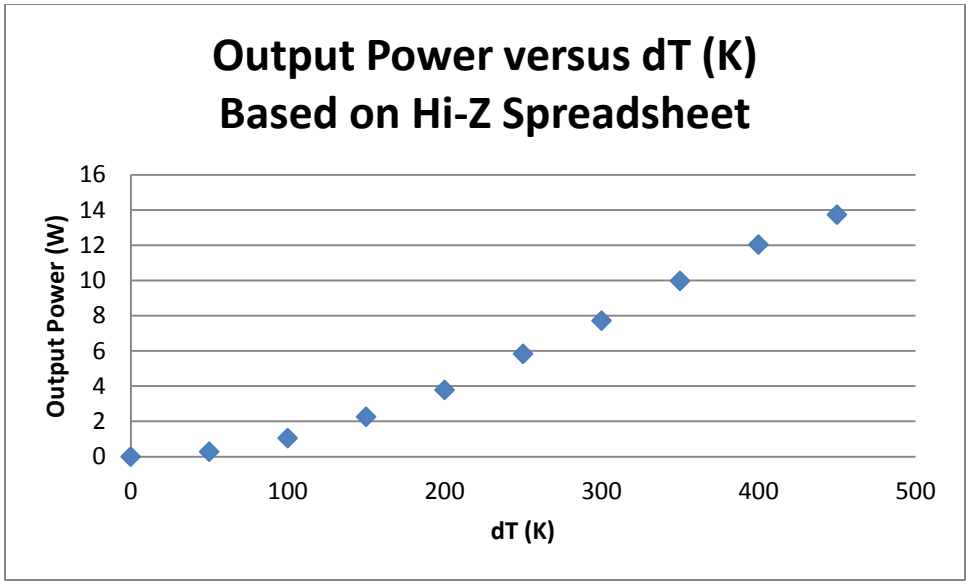

Figure 4.1: Hi-Z spreadsheet estimates for module output power versus temperature difference, assuming matched load impedance. The cold side temperature is fixed at 300 K. They note that the module is not designed to operate beyond 573 K (dT of 273K).

prepared from there. Based on a spreadsheet provided with the TE module, Figure 4.1 was assembled to evaluate what output power should expect to see from the module, based on the temperature difference. With this table in mind, along with a similar table for internal resistance versus temperature, the output power of the module was measured as a function of internal resistance, assuming a temperature difference around 350 K with a 25 inch diameter mirror. The optimal power for this system was determined by connecting a potentiometer in series with the thermoelectric module. Figure 4.2 below shows how the power dissipated across the load changed as the potentiometer resistance was adjusted. A peak of 0.28 watts was observed when the

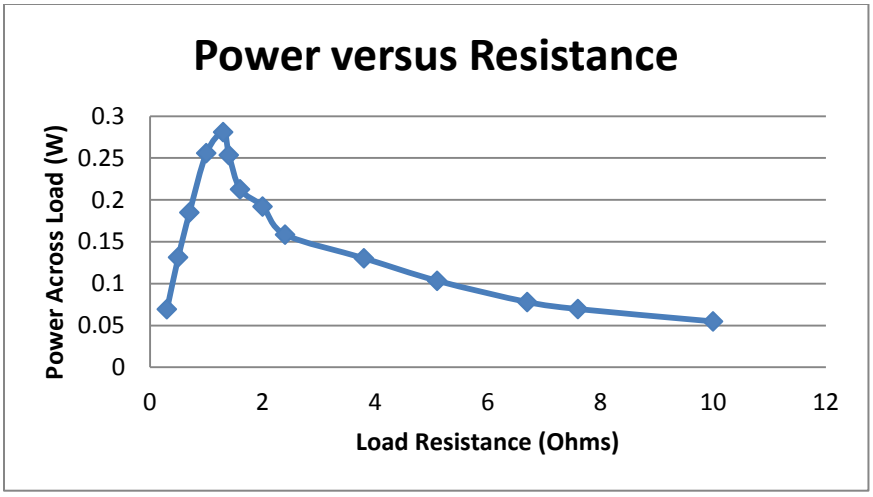

Figure 4.2: Power dissipated across potentiometer load versus load resistance. Peak power of 0.281 Watts found at 1.3 Ohm resistance. Mirror input power was 360 Watts (25 in diameter mirror).

load resistance was set to 1.3 ohms. These values are much different than the expected 9.98 Watts across a matched resistance of 0.884 ohms at 350K temperature difference. It seemed that the discrepancy was too large to be explained by the excess operating temperature

Several problems existed with the receiver setup as it was. First, the module was operating at a much higher temperature than the module was designed to function at. Either the input power needed to be reduced (the mirror) or the receiver needed to reduce the temperature more prior to arriving at the module (thicker insulator layer). Secondly, it was difficult to evaluate the accuracy of the copper heat spreader temperature because of the measurement dependence on the spot location. The thermocouple was placed slightly off center of the heat spreader, however, the

Figure 4.3: Pictures of the first generation solar receiver before and after heating. Right image shows the localized damage caused by the intensely concentrated solar irradiation on the copper heat spreader.

temperature read by the thermocouple could vary by as much as 200 degrees Celsius, depending on the proximity of the focused spot to the thermocouple. Regardless of the spot location with respect to the thermocouple, the produced module voltage output remained relatively constant in each test. It became impossible to determine what hot side temperature to use for calculations.

The temperature non-uniformity was further confirmed after removing the receiver from the system. It was observed that the copper not only became discolored at the location where the solar spot had been, but also there was obvious warping taking place due to the high temperature. This warping caused the copper to bend inward and crack the insulating ceramic layer. Figure 4.3 above shows the non-

uniformity of the damage done to the receiver. The temperature profile could be made more uniform if the copper heat spreader were to be thicker.

Finally, the spot size was not as nicely uniform as desired. A majority of the concentrated power was located in the top right corner of the heat spreader, with substantially less incident power across the rest of the receiver. This incident power non-uniformity was likely due to poor alignment of the system. With these issues in mind, we turned to ANSYS to try and determine how best to improve my setup.

4.2. ANSYS Simulations

In order to make constructive changes to the receiver, it was first important to simulate what we observed with the first receiver. According to the thermocouple on the copper heat spreader, the local temperature near the solar spot was around 700K and it could vary by as much as 500K. First, we wanted to look at how well the temperature spread through the receiver. If the temperature profile on top of the module was not uniform, its output power would be greatly impeded. So we constructed a virtual module that was 6.2 cm by 6.2 cm in surface area, with a 0.8 mm thick copper layer with 400 W/mK thermal conductivity, on top of a 0.8 mm thick insulating layer with 5 W/mK thermal conductivity, in attempt to reproduce the temperature map on the receiver with these dimensions. Figure 4.4 below shows the temperature profile on the top surface of the TE module assuming 307 W of incident power, after spreading through the copper and insulating layer. We can see that the maximum temperature is around 575 K and does not spread uniformly across the

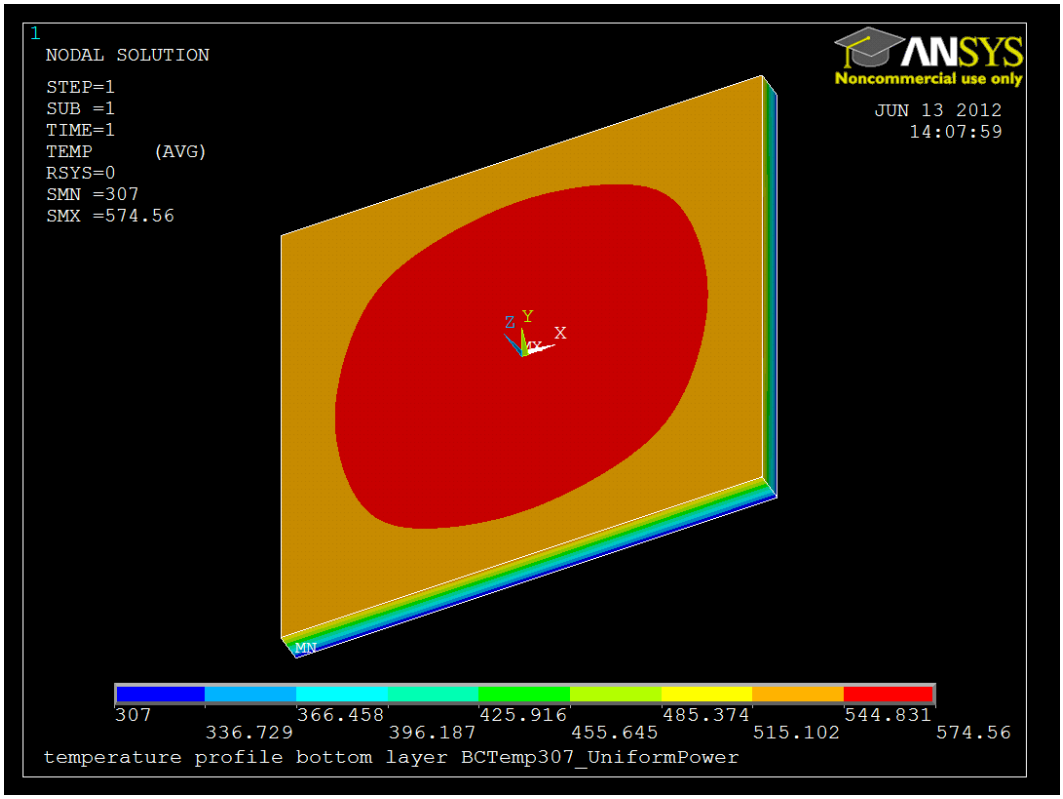

Figure 4.4: ANSYS simulation for uniform power temperature profile. Simulation shows the temperature profile on the thermoelectric module with 307 Watts of power uniformly distributed on top copper layer. Assumes 0.8 mm thick copper and 0.8 mm thick ceramic on top of module.

entire module. This informed us that even with ideal solar concentration, the receiver would need a thicker copper heat spreader to improve uniformity, in addition to a thicker insulating layer to reduce the temperature of the hot side of the module to non-damaging levels.

The second simulation we performed was trying to determine how the solar spot was distributing the energy on the heat spreader to cause a temperature range

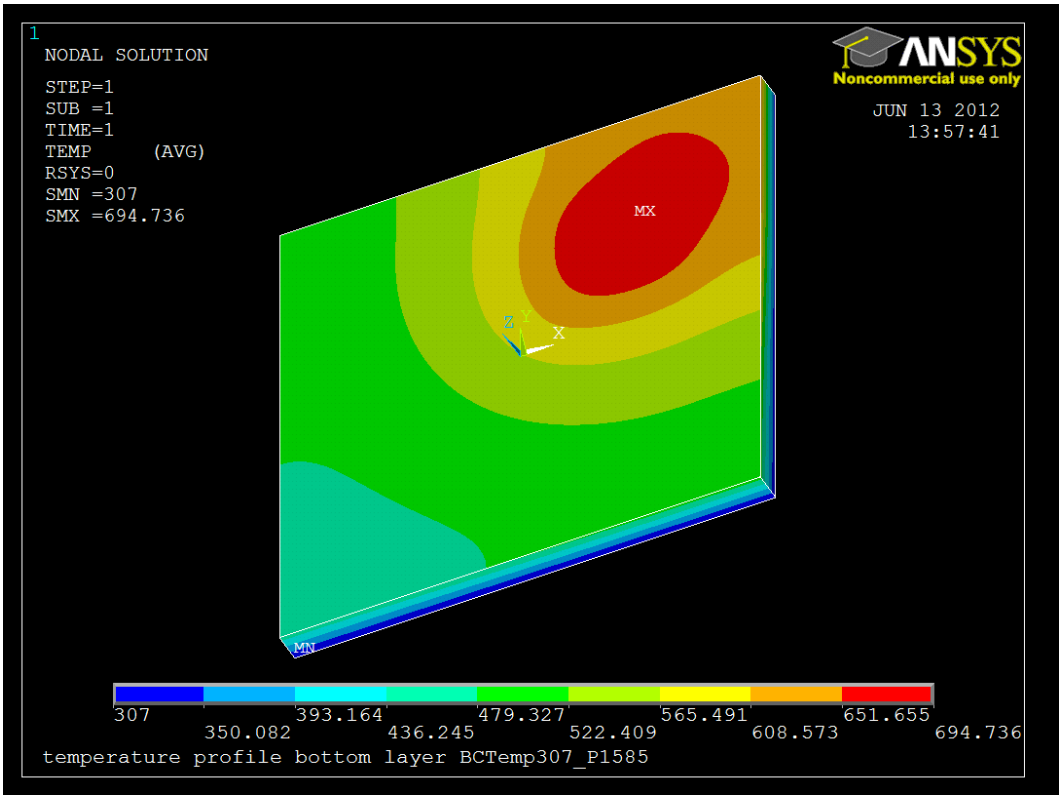

Figure 4.5: ANSYS simulation for 85-15 temperature profile. Simulation shows the temperature profile on the thermoelectric module with 307 Watts of incident power, with 85% of incident power in the top right quadrant and the other 15% distributed uniformly across the rest of the surface. Assumes 0.8 mm thick copper and 0.8 mm thick ceramic on top of module.

from 500-700K across the heat spreader. Visually, a majority of the incident energy was in one corner of the receiver with a small amount of energy sparsely spread across the rest of the receiver. So, we decided to have several power distributions to find what best explained my observations. After several simulations, we found that the correct temperature distribution occurred when 85% of the incident power was confined to one quadrant of the receiver, while the remaining 15% of the power was

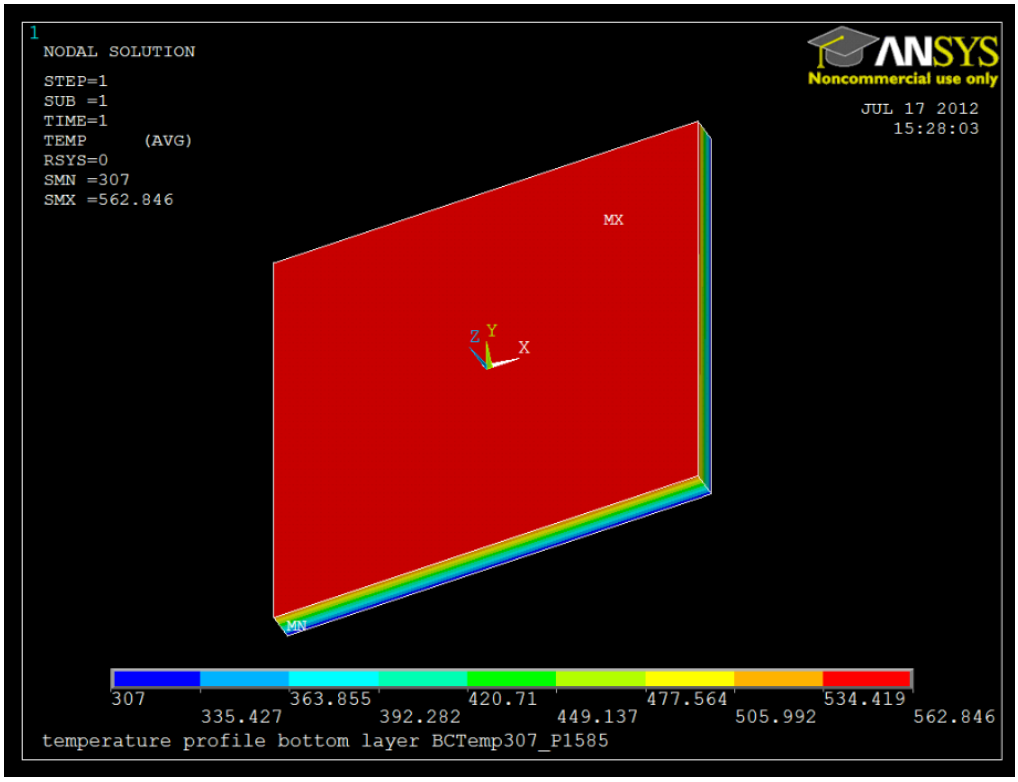

Figure 4.6: ANSYS simulation for 85-15 temperature profile with thicker top layers. Simulation shows the temperature profile on the thermoelectric module with 307 Watts of incident power, with 85% of incident power in the top right quadrant and the other 15% distributed uniformly across the rest of the surface. Assumes 6.0 mm thick copper and 6.0 mm thick ceramic.

evenly distributed across the rest of the receiver, as shown in Figure 4.5. The peak temperature was as high as 700K, with the furthest point from the hot spot being around 450 K.

Now that we had a clear idea of what our power distribution was, we began to adjust the thickness of both the copper heat spreader and the insulating ceramic to determine what we needed to prevent overheating and non-uniformity. As shown in

Figure 4.6, we were able to achieve a uniform operating temperature of 535 K across the whole module when the copper and insulator were both 6 mm thick, despite having the incident energy distributed so non-uniformly. These adjustments to the layer thickness would allow for additional measurements to be taken without compromising the various components from overheating.

4.3. Second Generation Receiver

After determining the needed receiver dimensions from the While the copper block with the desired dimensions was easy to find at the Baskin Engineering machine shop, the insulator was more difficult to acquire. All of the easily altered ceramic blocks all had a thermal conductivity around 0.3 W/mK, whereas the simulations used a 5 W/mK insulator. Instead of repeating the simulations for the alternate thermal conductivities, I was able to contact a company called Intermark that manufactures bulk quantities of thermal insulation pads. Fortunately, they had an insulating pad that had a 5 W/mK thermal conductivity and they provided a small piece of the desired thickness. A new TE module from Hi-Z was purchased to make sure that the previous device was not permanently damaged. With the new receiver now assembled, several of the measurements performed with the previous receiver design were repeated with the new receiver. Figure 4.7 shows the power dissipated across a load when placed in series with the module. The blue curve shows the original data for the first receiver, while the red curve shows the new data with the second receiver. An optimal power of 0.45 W was observed at 0.75 Ohms. The

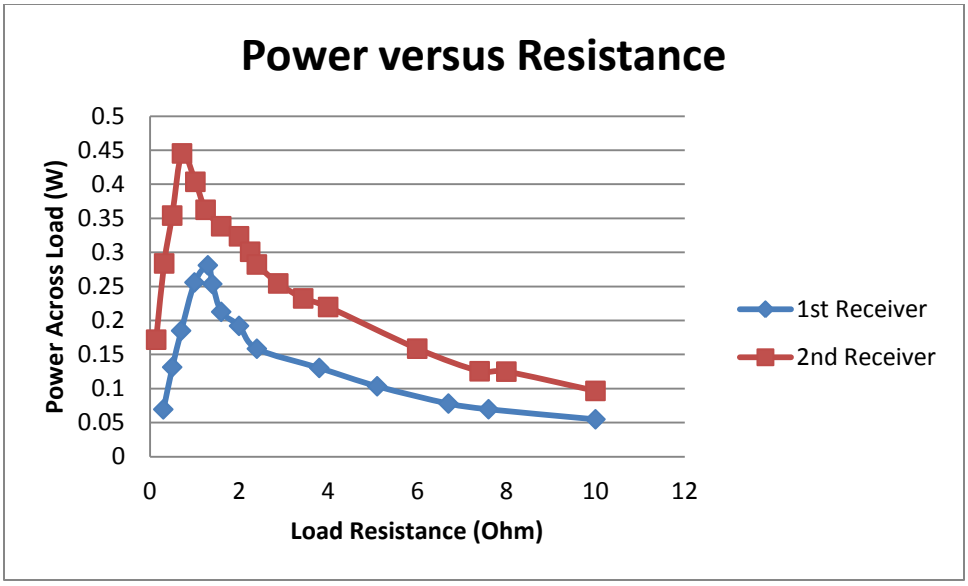

Figure 4.7: Power dissipated across load versus load resistance for both receivers. A peak exists when the load resistance matches the module internal resistance. The blue curve shows a peak of 0.28 W at 1.3 ohms for the first generation receiver, and the red curve shows a 0.45 W peak at 0.75 ohm for the second generation receiver.

second receiver performed better than the original by 60%. While this does seem like a substantial improvement, the performance is still substantially lower than advertised by the module manufacturer. Since three devices of the same model were measured, all producing approximately the same output power, it is likely that the module is not as powerful as the manufacturer thinks. If future research were to be performed on this system, it would be useful to evaluate the output of other TE modules to see how they compare.

Regardless of the relatively low electrical power produced by the module, the modifications made to the second generation receiver greatly improved the thermal

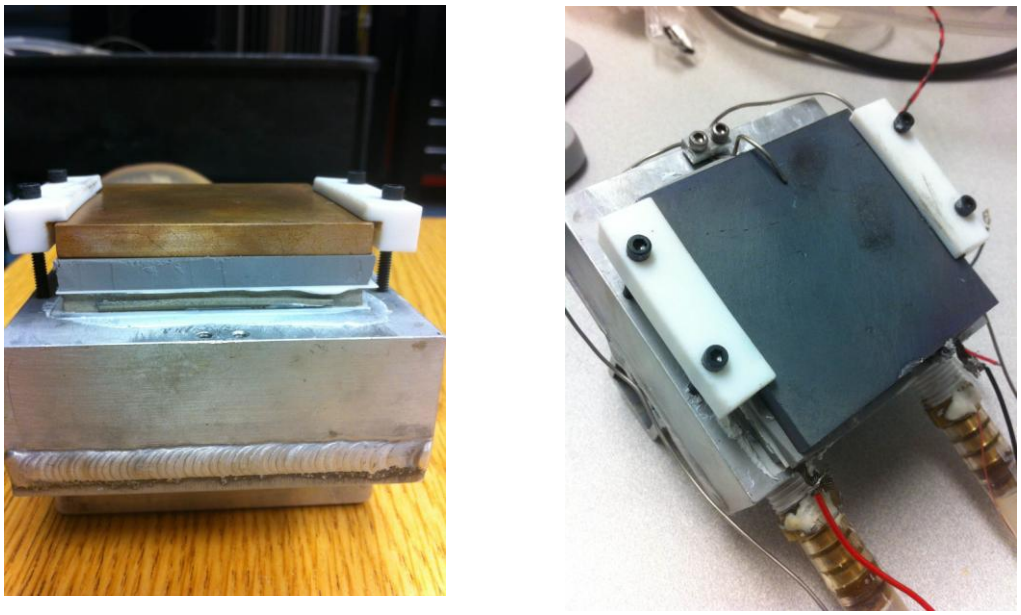

Figure 4.8: Second generation receiver before and after testing. The right image (after) was under concentration for several consecutive hours. The heat spreader damage is much more uniform as compared to the first generation heat spreader, showing the new design spread the temperature much better than previously.

functionality of the receiver. The first observation to be made was that the module heated up substantially slower than the original receiver, implying that the changes in temperature were much more gradual, which assisted with the lifetime of the heat spreader. Figure 4.8 above shows the second generation receiver before and after testing. The copper heat spreader has been discolored from remaining at 480 K for an extended period of time, however the uniformity of the discoloration was much better as compared to the damage shown previously for the first receiver. The module was able to repeatedly produce the same output voltage, demonstrating that the insulating pad dropped the operating temperature below destructive levels. The system modifications have been very useful in extending the testing time well beyond the

first receiver, in addition to preventing damage to the various components from overheating.

4.4. **Dish Size**

When deciding what size dish should be used for the system, we had to carefully consider the thermal resistance of the receiver. By knowing the thermal resistance, we could estimate how much incident power would be required to attain a given temperature. To determine how much the concentrated power will increase the temperature of the receiver, the following equation was used:

$$\Delta T = Q * Rth = (L/AK) * Q$$

where Q is the incident power on the receiver from the dish, L is the thickness of the receiver, A is the surface area of the receiver, and K is the thermal conductivity of the receiver. The incident dish power can be determined by examining the dish area, and comparing that area to the average solar power density, which was around 1.1 kW/m^2. The dishes that we purchased are advertised as being 97% reflective. Additional accuracy could be tested for if a solar meter could be acquired to verify the incident solar energy, as well as performing reflectivity tests to check the mirror's reflectivity.

Originally, the project was going to use a 35 inch diameter parabolic mirror to maximize the temperature difference across the module. However, this was a poor

choice that did not consider the maximum operating temperature of many components of the setup. The incident solar power on the dish was 600 watts, which ends up translating to an average operating temperature around 850K on the first generation receiver. Unfortunately, most of the receiver hardware is only rated for brief operation at 550K, such as the Delrin sample clamps, the thermoelectric module, and the water cooling tubes. To try and reduce the output power of the dish, a white bed sheet was used to cover a percentage of the dish. A yard stick was used to measure the dimensions of the revealed section of the mirror for calculating the area of incident solar energy.

After working with the large dish for several measurements on the first generation receiver, the dish broke off of the frame from a sudden alignment shift. The mirror was damaged and had to be replaced. Since the 35 inch mirror was too powerful, I decided to order a 25 inch mirror to replace it for future measurements, which only provided half the incident power at 307 watts. Based on the change in incident power, along with the thermal resistance of the first receiver, the heating was still as high as 700K. After upgrading to the second generation receiver, we would be able to uncover the entire dish and reach 480K average temperature, which is ideal for achieving a high temperature difference without compromising most of the receiver hardware.

4.5. Alignment and Spot Size

The alignment of the mirror and receiver system is very important for this experiment. If any part of the focused solar spot moves off of the receiver, the amount of incident power that heats the receiver will be reduced and it becomes extremely difficult to determine, which would make proper analysis difficult. It is also important to mount the parabolic mirror on the tracking frame in a way that minimizes any bending of the mirror. Since the mirror was not completely rigid, the mirror could wobble or bend from being touched or from being poorly mounted to the frame. If the mirror bends at all, the shape of the focused light spot on the receiver will be distorted. If the mirror is properly mounted and aligned with the sun, with the receiver placed a few inches from the focal point, the focused light will form a spot on the receiver with a high magnitude in the center, with a parabolically decreasing magnitude as the circular spot goes out radially. For predicting the change in performance with alignment, numerical calculation were performed with several assumptions. Using the ratio of the areas of the desired spot size to the 25 inch diameter dish, which has a focal point of 23 inches from the center of the mirror, it can be determined that a 3 inch diameter spot will exist at the center of the 6cm by 6cm square receiver when the receiver is located 18.5 inches from the mirror's center. The shift in spot size can be approximately equated to a change in the alignment angle of the mirror. Figure 4.9 shows the normalized open circuit voltage of the module as a function of the tracker misalignment, while considering the copper absorption coefficient of 0.65. The blue curve shows the theoretical expectation

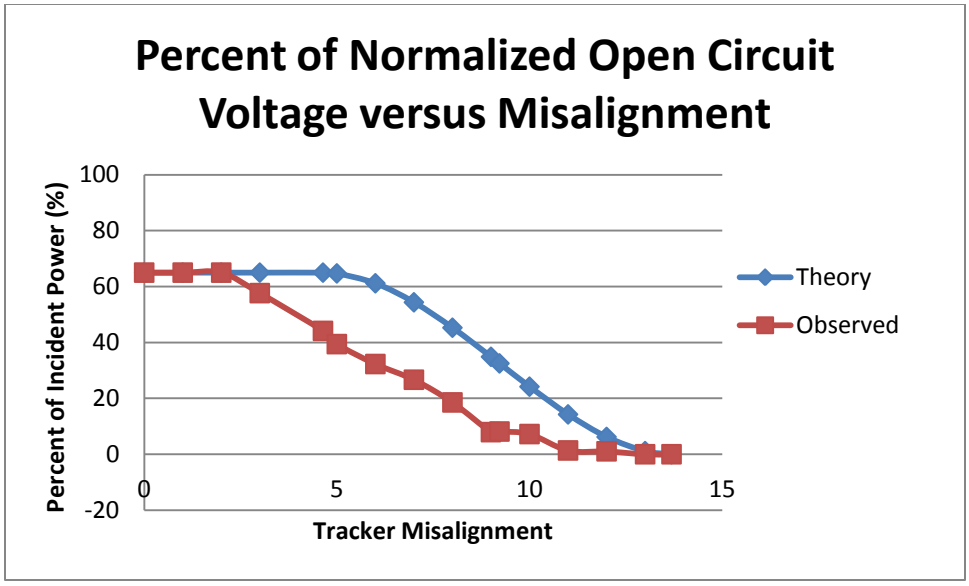

Figure 4.9: Effect of tracker misalignment on the system performance. Theory curve was generated assuming uniform spot shape. Observed behavior had much more abrupt changes, as the spot was not very uniform. In observed case, minimal changes in occurred when misalignment was within 2 degrees.

assuming a uniform solar spot. The red curve reflects the modules measured value, normalized by the open circuit voltage of 0.95 volts with no misalignment, and multiplied by the copper absorption coefficient of 0.65 to align with theory. The addition of the absorption coefficient does not take into consideration any secondary concentration from reflected light returning to the mirror to be reflected again. The theory suggests that any misalignment within 4.6 degrees should not affect the measurement, but anything beyond will begin to reduce the system input quite quickly. Due to the non-uniformity of the solar spot, a greater concentration exists at one side of the heat spreader than the other. Consequently, the misalignment has a greater effect on the incident power reduction at small misalignments and has a

smaller effect as the misalignment becomes greater. If the misalignment can be kept within 2 degrees, the incident energy is not reduced, which requires a small adjustment to the tracker once every few minutes. In the case of this setup, the tracking circuits used have shadow blocks that will respond to misalignment between 4.4 degrees and 17 degrees. Since this range was detrimental to the measurement, manual adjustments were made to keep the alignment within 2 degrees.

4.6. **Flow Rate**

The flow rate of the water cooling system has a critical role in regulating how much thermal energy is extracted from the system. As the receiver heats up, the water is in thermal contact with the aluminum heat sink, drawing heat energy away from the receiver by convection. If the flow rate is too high, the water will not be in contact with the water for a sufficiently long time to absorb any of the heat, so a slow flow rate is ideal for maximum heat collection. The thermal power transported by the heat pumping system can be explained by the following equation:

$$P = F * \rho * C * \Delta T$$

where P is the thermal power, F is the flow rate of the water in milliliters per second, ρ is the density of water (1 g/mL), C is the specific heat of the cooling fluid, which is 4.18 J/gK for water, and ΔT is the temperature difference between the water entering the heat sink and the water leaving the heat sink in degrees Kelvin. This number can be very high compared to the input power from the sun, as the system is not

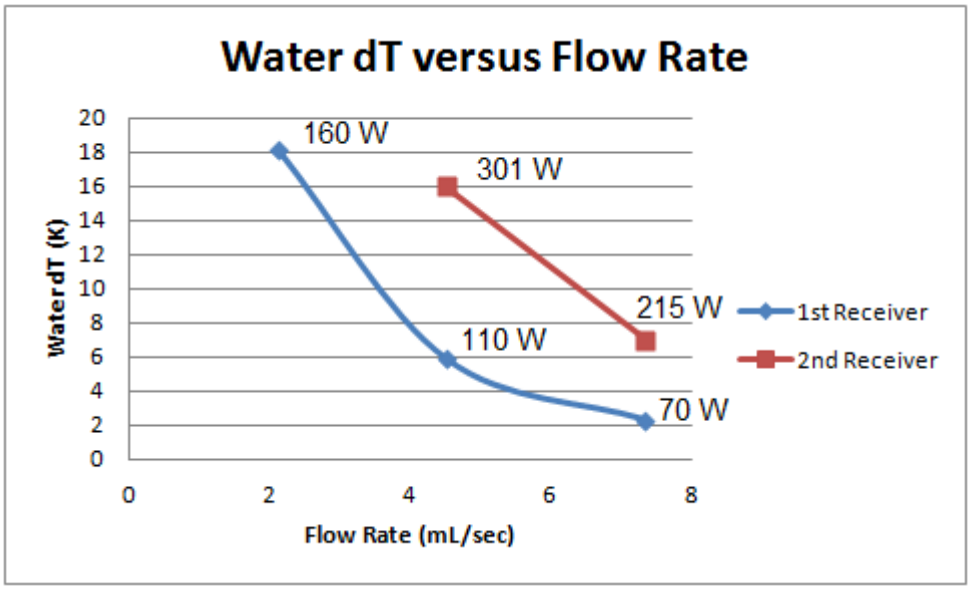

Figure 4.10: Change in water temperature versus flow rate for both receivers. Temperatures are measured at entry and exit of heat sink. The thermal energy for each flow rate is displayed next to each data point. Additional data from the second receiver could not be acquired due to temperatures getting too high with slower flow rates.

generating this energy, but rather, moving the heat around, as in a refrigerator. Figure 4.10 below shows the difference in water temperature between input and output as a function of the flow rate for the first generation receiver. The data in the graph corresponds to a closed loop water cooling system using the Zalman water pump and cooling tower. A closed loop cooling system continuously cycles the water through the heat sink and the cooling tower. This water pump is very powerful and naturally pumps at 8 milliliters per second. By bending and clamping the water path, the flow rate was able to be reduced as low as 2 milliliters per second, however any flow rate slower than that was not attainable without completely pinching off the entire flow. If

a weaker water pump were to be used, the amount of temperature difference achievable would likely be much greater. The blue curve corresponds to the first receiver, which could heat the water by 18 Kelvin with a flow rate of 2 mL/s. The second receiver was able to remain under solar exposure for a much longer time, and was able to sit at high temperature for a greater period of time. After reaching equilibrium around 480 K, the flow rates could be adjusted. At 4.5 mL/s, a temperature difference of 16 K could be produced across the heat sink, corresponding of a heat transfer of 301 watts. However, slower flow rates could not be measured with the second receiver due to the thermal insulation pad melting if the heat sink did not remove enough energy from the system fast enough. A more durable thermal insulator would be necessary to do additional examinations of the flow rate potential for thermal transport.

Additionally, the Zalman cooler is used as a heat sink for high performance computers, and is therefore not as ideal for thermal storage. An insulated reservoir would be more ideal for heat storage. In an ideally designed system, the cooling system would also be an open loop, where water was inserted via a large cold reservoir, and then pumped through the heat sink into an insulated hot reservoir for improved thermal storage. I attempted to perform measurements of the cooling potential of the system in an open loop, but my system was not designed in a way that could accommodate the measurement. The tracking frame is designed to hold the receiver at a greater height than I was able to position the Zalman cooling tower was. This makes it difficult for the water pump to function with an open loop, as the water

has to overcome an additional potential energy from the height difference. Additionally, since the cold reservoir is the storage tank of the Zalman tower, the flow rate of the pump will change based on how full the reservoir is, which changes relatively quickly in an open loop configuration. Maintaining a constant flow rate throughout the measurements would make accurate analysis very difficult to perform. For future work, larger water reservoirs would be very helpful for having a constant flow rate, in addition to reducing height differences between the receiver and the water pump.

4.7. **Heat Spreader Color**

To determine how absorbance is able to influence the potential of the system, black spray paint was applied to a copper heat spreader on the first generation receiver. Two separate copper heat spreaders were prepared for analysis: one with black spray paint coating the receiving side, and one without any spray paint. Measurements of open circuit voltage were taken within 20 minutes of each other to minimize the change in incident solar power due to the movement of the sun. This 20 minute time span was used for data collection, along with remounting time for the second heat spreader. Figure 4.11 below shows the open circuit voltages measured for each heat spreader. The peak points correspond to the steady state voltage produced by the TE module with each heat spreader. With the normal copper heat spreader, the module produced 0.9111 volts, while the same module with a black heat spreader

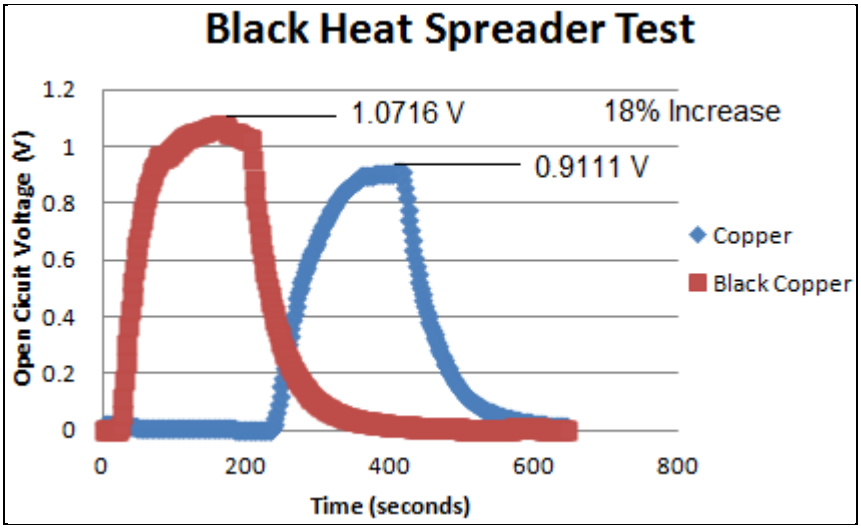

Figure 4.11: Effect of black heat spreader on system performance. Open circuit voltage output of the first generation TE module for two separate copper heat spreaders, one painted black and one unaltered. An increase in module output of 18% was observed.

produced 1.0716 volts. This translates to an 18% increase in performance due to the increase in absorbed light, and therefore heating. This improvement was less than the expected 40% improvement, based solely on the change of reflection coefficient from 0.65 of the dull copper to 0.92 for black spray paint. However, despite this noticeable increase in output voltage, the spray paint melted at the high operating temperature, causing it to run off of the module. The spray paint melting might account for why the expected system improvement did not occur. Since the spray paint will slowly melt off of the copper heat spreader because of the high temperatures that the system achieves, this system improvement does not practical to maintain over each temperature run. Each measurement would require a reapplication of the spray paint, which requires several hours to dry properly. Also, the average temperature of the

heat spreader was increased by around 50 degrees Celsius, where the system was already operating at close to maximum temperature without the painted heat spreader. It would be useful in the future to test a more thermally robust black paint that is designed to operate at much higher temperatures to see if additional heat could be collected on a more thermally robust receiver.

4.8. **Weather**

The weather has a very strong influence over the concentrator's ability to function. If the sun is covered by any clouds at all, the electrical voltage produced by the thermoelectric module is negligible. Figure 4.12 below shows an open circuit voltage versus time curve on the first generation receiver for a partially cloudy day. The two plateaus (regions I and III) correspond to time intervals where no clouds were blocking the sun. Region II shows the voltage produced when a white cloud (versus storm cloud) covered the sun for about a minute or two. The voltage generated dropped to an almost negligible value. This shows that this system is extremely limited by the weather. Even on partly cloudy days, the concentrators output will be compromised. As this data was collected in Santa Cruz, which has the Monterey Bay to the South, there were many days where I planned to take a measurement, but I was unable to due to frequent cloud movement blocking the sun. If this system were to be extended to larger scale production, it would have to be installed in a region of minimal cloud cover, such as arid or desert locations. Otherwise, the system would

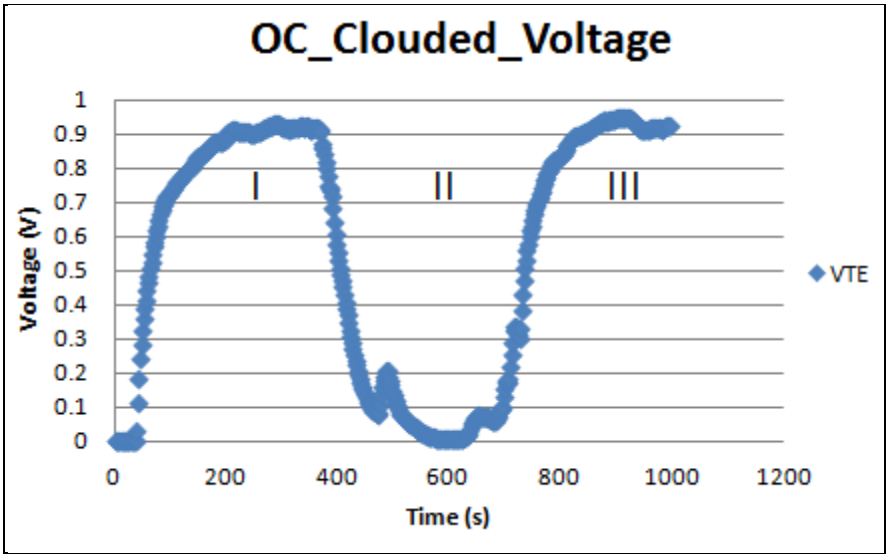

Figure 4.12: Open circuit voltage versus time on a cloudy day. Region II shows the minimal voltage output of the TE module when the sun is clouded over.

not be able to produce any appreciable power without totally sunny days, which is not a sustainable answer.

4.9. Overall System Performance

The efficiency of any working system can best be quantified by the ratio of the output of the system to the input. In the case of this setup, the output is measured by the amount of power extracted in the form of the electrical power generated by the thermoelectric module, combined with the thermal power transferred by the water cooling system. As discussed in the previous sections, the greatest performance of both features combined was with the second generation receiver at 0.45 watts of

electrical power with 301 watts of thermal power transferred. The inputs for the system include the incident solar energy on the dish that is refocused onto the receiver, in addition to the power required to run the water pump, tracking circuits, and flow meter. The tracking circuits each consume approximately 0.15 watts of power, the water pump uses around 1.5 watts, and the flow meter uses around 1 watt. The area of the parabolic mirror has about 384 watts of incident solar power that is reflected back to the receiver, depending on the time of day, after considering 97% reflectivity of the mirror. In total, the efficiency can be found as:

$$Efficiency\ \eta = \frac{Output}{Input} = \frac{0.45\ W + 301\ W}{384\ W + 0.3\ W + 1.5\ W + 1\ W} = 78\%\ Efficiency$$

On the surface, this efficiency may seem very high. The electrical power is generated by the module, however the thermal power is merely transported, as in a refrigerator, which has its efficiency measured as a coefficient of performance, which can be quite high. The system could be additionally insolated to ensure that more of the thermal energy is retained during transport. There is large amount of hose surface area that dissipates heat along the way.

The more important thing to examine is the underperformance of the TE module. According to the spreadsheet produced by Hi-Z Technologies, the module should be able to produce 3 watts of power across this load with a temperature difference of 250K across it. This performance is only 15% of expected output. As the overheating and temperature non-uniformity of the receiver has been fixed with the second generation receiver specifications, the likely origin of this

underperformance is attributed to either false calculations by the manufacturer, a faulty device, or poor thermal impedance matching. However, since three different modules were used over the course of the experiment, all of which showed similar results, a defective device is not very likely unless that particular module model was defective. Upon investigating the spreadsheet more closely, they do seem to include random enhancing factors to their formulas to make the data come out higher than expected. For example, when reporting the output power of the module across a matched load, they used the open circuit voltage instead. Regardless of the discrepancy between my observed output and the boasted output, the power generated is still minimal compared to the amount of power transported by the heat pump system. It would be useful to do thermal network analysis to see if the electrical power output is impeded due to irregular heat flow within the module. If there is a non-uniformity in the thermal behavior, it could cause the module to underperform, as we are seeing.

4.10. Error Analysis and System Improvements

If I were to continue working with this system to try and improve the combined cogeneration output of this system, there are several changes that should be made to the system to improve its performance. First, there are several flaws in the tracking system that made it cumbersome to work with. For example, the design of the tracking plates is not very robust. All of the weight rests on a comparatively small joint controlled by a motor. If large changes were made to the alignment of the frame,

there was obvious strain in the motor system. Reducing torque and adding additional support in the tracking plates would greatly improve the tracking reliability and lifetime. The motors that controlled the tracking motion had gear reduction installed to reduce the strain on the motors. However, the gear reduction is very high such that the tracking frame takes a very long time to make changes. If the system were unmanned and operated, it would probably be fine, but since I was constantly monitoring the system, it became very cumbersome. Also, as mentioned previously, one of the axes tracked the azimuthal angle instead of the horizontal angle, which is much more important for tracking, and a corrected design was suggested. That design should be assembled and installed to correct the tracking accuracy.

Further improvement could be made to the thermocouple system for more thorough temperature information. The best solution would be to install an array of thermocouples on the surface of the copper heat spreader. While the temperature profile seemed uniform across the copper surface as I checked it manually, this could be confirmed with additional thermocouples reading real time values. This could give a much better idea on the temperature uniformity across the heat spreader at all times during the measurements. However, different computer interfacing would be necessary to read that many thermocouples. Each TC-01 thermocouple reader used a separate USB slot on the data collection computer. Omega Engineering manufactures an eight channel thermocouple USB reader that would be better suited for working with more thermocouples.

Additional improvements would be necessary for the water cooling and thermal storage system as well. First, it would be prudent to use an insulated hot side reservoir so that the thermal energy could be stored for a prolonged period of time. The Zalman tower/pump was a good dual-purpose device. However, its design is focused around dissipating heat energy, which is good for a closed loop testing system, but not optimal for a commercial system. The closed loop system does offer an accurate representation of how well the heat energy can be pumped away from the receiver, but additional information about storing the thermal energy afterward cannot be done with this pump. Additionally, if the system were to be made into an open loop system where the water was not continuously cycled, it would require that the tracking system support tripod be lowered or removed so that whatever pump is used would not have to overcome the additional potential associated with the receiver height. By having the water pump located above the receiver, the pump would not have to work as hard to get a continuous flow. It would also be useful to reduce the pumping speed of the water pump. This would give the water passing through the receiver more time to collect and transport the heat energy from the system. However, this would also reduce the temperature difference across the TE module, causing its performance to be reduced. Since a majority of the system output comes from transporting the heat energy versus generating the electrical energy, the overall system improvement would be greater if the thermal transport was favored over the electrical output.

5. Summary and Conclusion

A solar tracker and concentrator was designed and assembled for the purpose of cogeneration of thermal power and electrical power using thermoelectric technology. A thermoelectric module was placed between the concentrated sunlight and a water cooling system to produce electrical power from the temperature gradient. The system was tested to see if there was a place for thermoelectric devices to be used in conjunction with solar thermal systems. The system was able to transfer as high as 78% of the incident 384 watts of thermal energy from the sun via the water cooling system, but was not able to produce a substantial amount of electrical power with the thermoelectric. Several TE modules were tested during various stages of the project, but they all performed at 15% of their expected output of 3 watts. Either the modules were not as powerful as advertised or the thermal impedances of the various layers within the receiver were not well matched for optimal heat transport. The closed loop coolin\g system worked well to display how well the water cooling can extract thermal energy from the receiver, but the system was not designed for optimal thermal storage after extracting the heat. Many improvements to the system were made in order to prevent overheating from damaging key components of the receiver.

If further investigation was performed, it would be useful to examine alternate TE modules for determining if thermoelectrics can be used effectively in solar concentration systems. For the devices used in this project, the output was not very substantial at the receiver's operating temperature. Modules designed for working at

much greater temperatures would be much more beneficial for examining their potential output on these systems. In general, a more thermally durable receiver would be very important in large scale solar concentrators, where the receiver can reach temperatures up to 1000 K or higher. Additionally, using high absorption coatings would be beneficial for the system if the coating can withstand the high temperatures that the receiver endures. Improving the receiver absorption would have a great impact on the overall system efficiency. It would also be useful to optimize the location of the research. By moving the system to an area that receives more consistent sunlight throughout the year, it would allow for studies of the system performance over a longer duration. By implementing all of these additional system improvements, it would become much clearer whether or not thermoelectrics could provide an appreciable synergy to solar concentration systems.

6. References

1. ANSYS Inc. Theory Reference for the Mechanical APDL and Mechanical Applications. Release 12.1, November 2009. Pages 267-268, 979-980.
2. Bahk, J. et al. Thermoelectric figure of merit of $(In_{0.53}Ga_{0.47}As)_{0.8}(In_{0.52}Al_{0.48}As)_{0.2}$ III-V semiconductor alloys Physical Review B, vol. 81, Issue 23, id. 235209.
3. Chung, Deborah. Composite Materials: Science and Applications. 2nd ed., 2010. Page 237-245.
4. Dynamic Ceramics. Properties of Engineering Ceramics. Available Online: http://www.dynacer.com/thermal_properties.htm
5. Ecoworld. How Much Solar Energy Hits Earth?. Posted on 14 June 2006. Available Online: http://www.ecoworld.com/energy-fuels/how-much-solar-energy-hits-earth.html.
6. Engineering Toolbox. Coefficients of Linear Thermal Expansion. Available Online: http://www.engineeringtoolbox.com/linear-expansion-coefficients-d_95.html
7. Green, Martin. *Third Generation Photovoltaics*. Springer, 2003. Available Online: http://www.amazon.com/dp/3540265627/ref=rdr_ext_tmb#_
8. Hicks, L. D., and M. S. Dresselhaus. "Thermoelectric figure-of-merit of a one dimensional conductor." Physical Review B 47 (1993): 16631-16634.
9. Index Mundi. United States Crude Oil Consumption by Year. Available Online:

http://www.indexmundi.com/energy.aspx?country=us&product=oil&graph=consumption

10. Kasap, S. O. Principles of Electrical Engineering Materials and Devices. Third Edition. Boston: McGraw-Hill, 2006.
11. LTP. Calculating the Energy from Sunlight over a 12-Hour Period. Available Online: http://www.grc.nasa.gov/WWW/k-12/Numbers/Math/Mathematical_Thinking/sun12.htm
12. Omer, Siddig and Infields, David. Design and thermal analysis of a two stage solar concentrator for combined heat and thermoelectric power generation. Energy Conversion & Management 41 (2000) 737-756
13. Richmond, P. E. The Peltier effect. 1966 Phys. Educ. 1 145. Available Online: http://iopscience.iop.org/0031-9120/1/3/301
14. Rowe, D. M., ed. Thermoelectrics Handbook: Micro to Nano. Florida: Taylor & Francis Group, 2006.
15. Shakouri, Ali. Recent Developments in Semiconductor Thermoelectric Physics and Materials. Annual Review of Materials Research. Vol. 41: 399-431. August 2011.
16. Snyder, G. and Toberer, Eric. Complex thermoelectric materials. *Nature Materials* **7**, 105 - 114 (2008). doi:10.1038/nmat2090.
17. Solar Thermal Technology on an Industrial Scale. Available Online: http://www.solar-thermal.com

18. Tan, J. et al. Thermoelectric properties of bismuth telluride thin films deposited by radio frequency magnetron sputtering. Proc. SPIE 5836, 711 (2005).
19. TE Technology Inc**.** Frequently Asked Questions on Thermoelectrics. Available online**:** http://www.tetech.com/FAQ-Technical-Information.html
20. Venkatasubramanian, Rama, et al. "Thin-film thermoelectric devices with high room-temperature figures of merit". *Nature* **413** (6856): 597–602. 2001
21. Yazawa, Kazuaki and Shakouri, Ali. Cost-Efficiency Trade-off and the Design of Thermoelectric Power Generators. *Environ. Sci. Technol.*, 2011, *45* (17), pp 7548–7553 Available Online: http://pubs.acs.org/doi/full/10.1021/es2005418
22. Yazawa, Kazuaki and Shakouri, Ali. Energy Payback Optimization of Thermoelectric Power Generator Systems. IMECE2010 November 2010. Available Online: http://quantum.soe.ucsc.edu/sites/default/files/IMECE2010-yazawa.pdf
23. Yazawa, Kazuaki and Shakouri, Ali. System Optimization of Hot Water Concentrated Solar Thermoelectric Generation. ThETA 3, Cairo, Egypt, Dec 19-22nd 2010. Available Online: http://quantum.soe.ucsc.edu/sites/default/files/yazawa_theta2010.pdf